Chapter 3

# Recent Progress in Synthesis of Nano- and Atomic-Sized Catalysts

**Krishnapriya Ramachandran, Unnati Gupta, Divya Kumar, Devika Laishram, and Rakesh K. Sharma***

**Sustainable Materials and Catalysis Research Laboratory (SMCRL), Department of Chemistry, Indian Institute of Technology Jodhpur, Jodhpur 342037, Rajasthan, India**

***Email: rks@iitj.ac.in**



Well-defined nano- and atomic-sized heterogeneous catalysts with extremely high catalytic activities and unique selectivities show promise in addressing the critical energy- and environment-related challenges of this century. The exceptional properties of these catalysts, such as their electronic and geometric structures and the effective interactions between metals and supports, give rise to unprecedented catalytic efficiency over that of conventional catalysts. The facile prospects for tuning the active sites of these catalysts pave the way to optimizing their activities, selectivities, and stabilities, thus offering extensive application possibilities in significant industry-related catalytic reactions. A prerequisite for synthesizing nano- and atomic-sized catalyst is to prepare extremely disperse nano- and subnanoscale atoms on suitable supports. This book chapter summarizes various synthesis methods employed to synthesize nano- and atomic-scale catalysts.

## 1. Introduction

Heterogeneous catalysis involving supported metal nanostructures is widely used in many industrial processes, such as biomass conversion, water splitting, fuel-cell operation, ammonia synthesis, and $CO_2$ reduction (*1*). Downsizing the metal particles to the subnanometer regime allows enhanced catalytic properties by improving the surface-to-volume ratio, facet-dependent activity, and surface-atom coordination to the catalytically active regions. Materials with dimensions between 0.1 and 100 nm are referred to in the literature as nanoparticles, nanoclusters, or nanocrystals. Generally, nanomaterials with diameters in the range of 2.0–100 nm are called nanoparticles (NPs), and if the diameter falls below 10 nm, they are called nanodots. Quantum dots are a special class of fluorescent nanodots consisting of tiny nanocrystals of semiconducting materials with diameters in the range of 2–10 nm. Because of their small size, the electrons in these particles are confined, and the radii of the semiconductor nanocrystals are smaller than the exciton Bohr radius with quantization of the energy levels. Particles with sizes smaller than 2.0 nm are termed nanoclusters (NCs). On the


Sudarsanam and Singh; Advanced Heterogeneous Catalysts Volume 1: Applications at the Nano-Scale
ACS Symposium Series; American Chemical Society: Washington, DC, 2020.

other hand, tiny particles having core sizes of less than 1.0 nm can be distinguished as subnanometer clusters (SNCs) (*2*). SNCs are composed of fewer than 50 atoms and have sizes of less than 1 nm, which is comparable to the Fermi wavelength of the electron (*3*). Thus, SNCs are considered to be an intermediate state between single atoms and metal NPs of greater than 1 nm (*4*). The tuning of bulk materials into NPs, SNCs, and finally single metal atoms leads to increased unsaturated coordination, which results in an increase in the surface free energy of the individual metal components. This results in enhanced chemical interactions, so that the metal sites become highly catalytically active, thus increasing the effective atom-utilization rate (*5*). This size effect of nanocatalysts is illustrated in Figure 1.

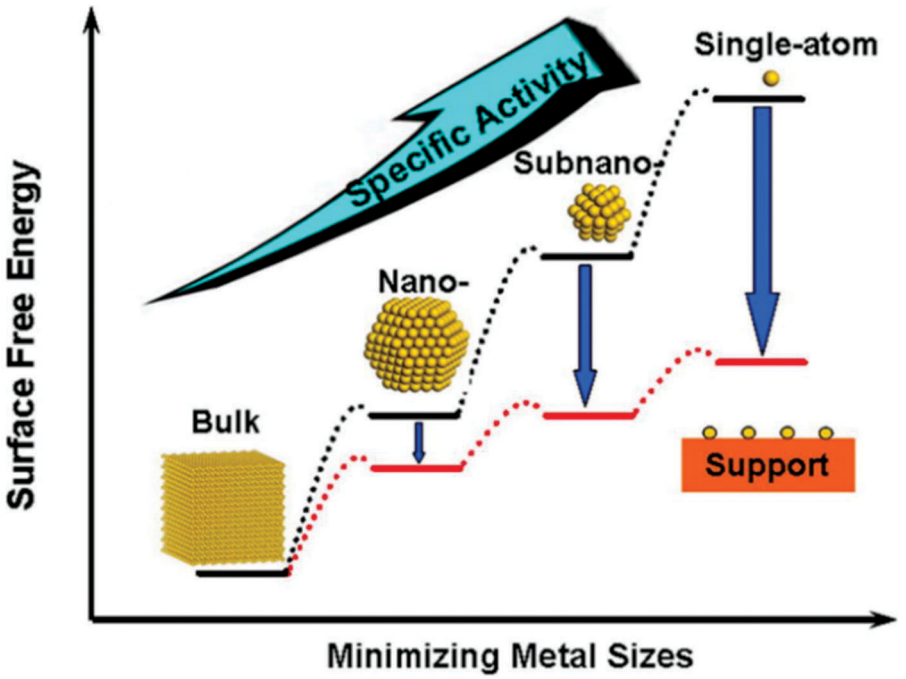


*Figure 1. Schematic of changes in surface free energy and specific activity per metal atom with metal particle size and support effects on stabilizing single atoms. Reproduced with permission from reference* (*5*). *Copyright 2013 American Chemical Society.*

With advances in synthesis and characterization techniques and electronic technology, NPs with core sizes even smaller than l.0 nm can be effectively captured and characterized. However, the fabrication of such SNCs is a major challenge, as the undercoordination and electronic accessibility of metal atoms in SNCs makes them highly reactive, which leads to thermodynamic instability. The stabilization of SNCs can be achieved by protecting ligands in solution or by providing support to the SNCs on solid organic or inorganic matrixes (*1*). At high temperatures, these SNCs become more mobile and vulnerable to agglomeration, because of their higher surface energies (*6*). Several methods such as soft-landing techniques, wet chemistry methods, and atomic dispersion of the metal species on supports can be employed to synthesize these nanocatalysts (*2*, *7*–*9*). This book chapter intends to summarize recent advances in various traditional and new synthesis strategies applied to the fabrication of nano- and atomic-sized catalysts.

## 2. Synthesis Methods for Nano- and Atomic-Sized Catalysts

The size-controlled synthesis of nano- and atomic-sized catalysts is very challenging. Two strategies are mainly used for the precisely controlled synthesis of NCs: bottom-up and top-down. The bottom-up approach uses the reduction of the metal ion precursors by suitably weak or strong reducing agents with the help of appropriate ligands, followed by nucleation of the reduced metal atom. The nucleation process is controlled precisely by varying the quantities of reducing agents or the amounts of protective ligands or by changing the solvents. In contrast, in the top-down approach, NCs are synthesized from larger NPs by core-etching or size-reduction methods.

### 2.1. Bottom-Up Approaches

#### *2.1.1. Brust–Schiffrin Synthesis*

Brust–Schiffrin synthesis is a bottom-up synthesis method for fabricating Au NCs through the biphasic (water/toluene) reduction of $AuCl_4^-$ (*10*). This method is recognized as a simple approach to the direct synthesis of surface-functionalized metallic clusters, specifically, the preparation of Au NCs in an organic liquid. Here, the metal precursor was dissolved in water, and a phase-transfer process was performed using a suitable phase-transfer catalyst such as tetraoctylammonium bromide (*6*, *11*). NCs containing 1–3-nm metal atoms were successfully prepared by adding the reducing agent (sodium borohydride) and the protecting ligands (alkanethiol) to the organic layer. This method is also known as the direct-synthesis method. The mechanism of formation of these NCs was first explained by Perala and Kumar (*12*), who proposed that, if the synthesis environment is unchanged, a continuous nucleation–growth–capping process occurs that results in the complete capping of particles devoid of further growth at the same size. In contrast, new particles can start growing continuously, causing highly monodisperse particles. A schematic representation of this growth mechanism is provided in Figure 2.

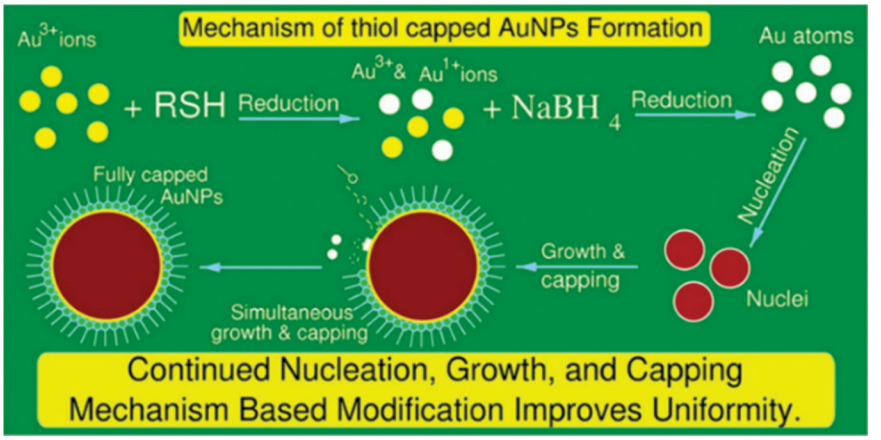


*Figure 2. Schematic of the proposed mechanism for Brust–Schiffrin synthesis. Reproduced with permission from reference* (*12*). *Copyright 2013 American Chemical Society.*

In 1995, Brust et al. modified the two-phase method into a one-phase method in which the reaction was carried out in a polar solvent (methanol or tetrahydrofuran) (*13*). By means of these methods, NCs of Au, Ag, Pt, Pd, and Cu with specific sizes have been easily prepared (*14*–*22*). Among the metals, the noble metal gold has been studied systematically owing to its stability under

ambient reaction conditions. The properties of the nanocrystals were controlled successfully by modifying the reaction parameters such as the ligand-to-metal ratio, the protective ligands, the concentrations of reactants, the use of weak or strong reducing agents, the temperature, the reaction period, and the pH of the solvent used. Zhu et al. (*23*) synthesized one-sized $Au_{25}(SR)_{18}$ NCs (where SR represents an alkyl- or arylthiol) by tuning the formation kinetics of the Au(I) intermediate species through parameters such as the stirring rate and temperature. Likewise, Wu et al. (*24*) presented a simple one-pot synthesis procedure for synthesizing $Au_{25}(SR)_{18}$ NCs using the tetrahydrofuran method by a distinct size-focusing approach. Their study revealed that, at extended reaction times, the initially formed polydisperse product was transformed entirely to a monodisperse species. Goulet and Lennox proposed a revised mechanism for the Brust–Schiffrin method based on a $^1H$ NMR study and suggested that, for the one-phase reaction, gold(I) thiolate is the main precursor, whereas for the two-phase method, a gold(I)–tetraoctylammonium halide complex is the chief precursor prior to the reduction process (*25*). Later, Li et al. (*26*) also confirmed the former mechanism with thorough studies using Raman and NMR analyses.

### *2.1.2. Phosphine-Capped Synthesis*

Phosphine-stabilized NPs are considered to be potential precursors to other functionalized NP building blocks containing well-defined metallic cores. Various reports on using amino-substituted triarylphosphine ligands to synthesize Au NCs were published earlier (*27*, *28*). This method received much attention after the report by Hutchison's group of a safer and more convenient synthesis of phosphine-stabilized Au NPs (*29*). The two-step, scalable synthesis of phosphine-stabilized NPs was achieved using sodium borohydride as a reducing agent. Initially, the hydrogen tetrachloroauric(III) acid trihydrate ($HAuCl_4{\cdot}3H_2O$) precursor was allowed to react with triphenylphosphine to yield 1 equiv each of $AuCl(PPh_3)$, triphenylphosphine, and triphenylphosphine oxide and 3 equiv of HCl. Afterward, the mixture was reduced with $NaBH_4$. Later, Wang's group (*30*) reported the $PPh_3$-protected synthesis of $Au_{20}(PPh_3)_8$ NCs using the above method. The synthesis involved the dissolution of $AuCl(PPh_3)$ and tetraoctylammonium bromide in a toluene/water mixture, followed by the slow addition of $NaBH_4$ aqueous solution with continuous stirring. However, the resultant clusters lacked a narrow size distribution (fewer than 12 Au atoms) and low yield. Diphosphine ligands can be used to obtain metal NCs with a narrow size distribution. For example, Bertino et al. (*31*) successfully synthesized monodisperse suspensions of ultrasmall tetrahedral $Au_{20}$ clusters $Au_N$ ($N < 12$) using the Au precursor $Au^{(I)}Cl(PPh_3)$ and the bidentate phosphine ligand $P(Ph)_2(CH_2)_MP(Ph)_2$. In their synthesis procedure, the Au precursor and ligands were first dissolved in an organic solvent, and then the Au(I) was reduced by the slow addition of a borane–*tert*-butylamine complex. $Au_{11}$ clusters were obtained with the use of $P(Ph)_2(CH_2)_3P(Ph)_2$ ligands, whereas $P(Ph)_2(CH_2)_MP(Ph)_2$ ligands with $M = 5$ and 6 yielded $Au_{10}$ and $Au_8$ clusters, respectively. In another interesting work, Pettibone and Hudgens (*32*) synthesized monodisperse NCs of distinct nuclearity by carefully controlling the ligand ratios ($0 \leq [ligand]/[PPh_3] \leq 18$). In a typical synthesis, $AuCl(PPh_3)$ and the ligand [1,6-bis(diphenylphosphino)hexane] were used as the Au precursor and ligand, respectively. The reduction of the metal was achieved with $NaBH_4$ in the 1:1 methanol/chloroform solution. Huang et al. (*33*) synthesized atomically monodisperse $[Au_6(PPh_3)_6]^{2+}$ NCs

in two distinct stages avoiding multistep conversions from $[Au_9(PPh_3)_8]^{3+}$ to $[Au_8(PPh_3)_8]^{2+}$ and then from $[Au_8(PPh_3)_8]^{2+}$ to $[Au_6(PPh_3)_6]^{2+}$, as shown in Figure 3.

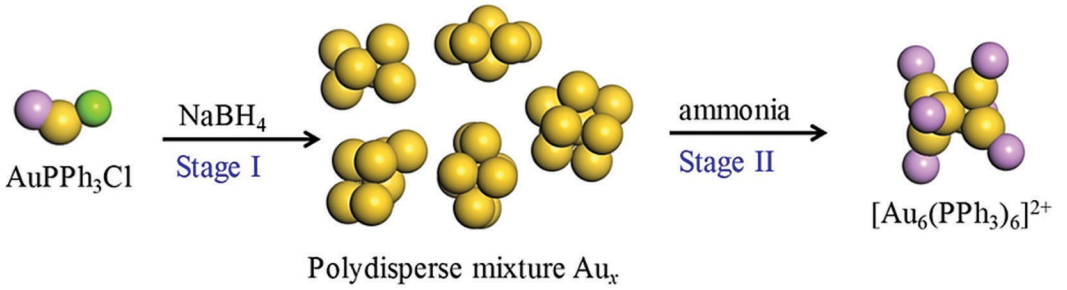


*Figure 3. Schematic illustration of the synthesis of atomically monodisperse $Au_6$ NCs using ammonia-induced size convergence. Reproduced with permission from reference* (33). *Copyright 2018 American Chemical Society.*

Figure 4 shows the first kinetic reduction stage, which resulted in the formation of narrowly size-distributed $Au_x$ ($x = 6, 7, 8, 9$, and 11) NCs. In the second stage, the NC mixture was size-converged into atomically monodisperse $Au_6$ NCs in the presence of aqueous ammonia. The uniqueness of this synthesis route is that the method can be applied to many protecting ligands such as thiols, amines, and even polymeric ligands. A simple, one-step synthesis of phosphine-stabilized Au NPs of narrow size dispersion (1.2−2.8 nm in size) was reported by Shem et al. using the mild reducing agent 9-borabicyclo[3.3.1]nonane (*34*). Au NPs of high purity were obtained depending on the reaction conditions and the phosphine ligand used, as seen in Figure 4a. Phosphine-protected monodisperse NCs of $[Au_{13}(dppm)_6](BPh_4)_3$, $[Au_{18}(dppm)_6Br_4](BPh_4)_2$, and $[Au_{20}(dppm)_6(CN)_6]$ [where dppm = bis(diphenylphosphino)methane] were successfully synthesized by the thiol and size-focusing route (*35*). $[Au_{18}(dppm)_6Br_4](BPh_4)_2$ was converted into $[Au_{13}(dppm)_6](BPh_4)_3$ and $[Au_{20}(dppm)_6(CN)_6]$ by the surface engineering of the ligands under $PPh_3$ or $NaBH_3CN$, as shown in Figure 4b.

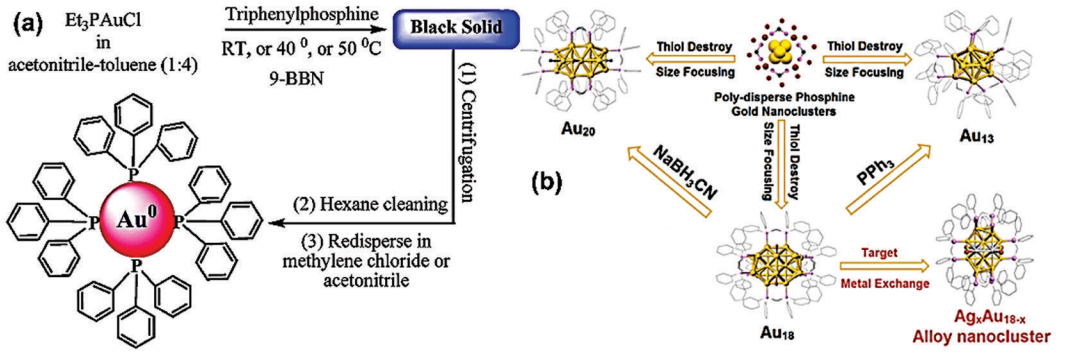


*Figure 4. (a) Synthesis pathway for phosphine-stabilized Au NPs. Abbreviations: 9-BBN, 9-borabicyclo[3.3.1]nonane; RT, room temperature. Reproduced with permission from reference* (34). *Copyright 2009 American Chemical Society. (b) Synthesis of atomically precise phosphine-capped gold NCs (with more than 10 metal atoms). Reproduced with permission from reference* (35). *Copyright 2017 American Chemical Society.*

*2.1.3. MOF-Derived Synthesis*

This is a bottom-up method that uses metal–organic frameworks (MOFs) to synthesize high-quality nanoscale catalysts. MOF-derived materials are synthesized from MOF-based precursors or templates. Such syntheses include a series of post-processing techniques such as thermal treatment, chemical modification, and surface decoration. The synthesis of MOF-derived materials basically involves two major steps: preparation of the selective MOF precursor in the first step and deliberate post-treatments in the second step. MOFs are composed of metal-containing nodes and organic linkers. Metals present in MOF nodes can be partly exchanged with further metals by the coordination environment provided by the MOF linkers, which facilitates the creation of a desirable spatial distance of metal sites. Through the selective removal of the doping atom and the aid of an in situ reduction process, supported single atoms or their clusters distributed on porous matrixes can be synthesized easily (*36*, *37*). MOF-derived nanoscale catalysts have the advantage of precise morphologies; ultrahigh porosities (up to 90% free volume); and huge internal surface areas, extending beyond 6000 $m^2/g$, as well as easy doping of heteroatoms, metal NPs, and metal oxide NPs. They exhibit large surface areas and can provide large amounts of active sites, and thus, they can be tuned as exceptional and robust heterogeneous catalysts, cocatalysts, or catalyst supports for many catalytic reactions (*38*). Li and co-workers prepared an MOF-confined pyrolysis strategy for the formation of highly concentrated Co isolated single atoms (ISAs) on a nitrogen-doped carbon support (*39*). This strategy was based on the high-temperature pyrolysis of predesigned Zn/Co bimetallic zeolitic imidazolate frameworks (ZIFs) to nitrogen-doped carbon (N-C). In this process, the addition of $Zn^{2+}$ replaced certain $Co^{2+}$ sites, and the $Zn^{2+}$ ions served as a fence for the spatial separation of $Co^{2+}$ ions. The lower-boiling-point Zn was selectively evaporated at a temperature higher than 800 °C, whereas the Co was reduced by carbonized organic linkers. This resulted in Co ISAs on the N-C support, establishing a new research regime on ISA materials on highly thermally stable carbon supports with high metal loadings. Furthermore, the same group also reported that the coordination number of single Co atoms could be tuned by varying the pyrolysis temperature (*40*). In this case, three atomically dispersed Co catalysts with different Co–N coordination numbers ($Co–N_4$, $Co–N_3$, and $Co–N_2$) were selectively prepared at 800, 900, and 1000 °C, respectively. Another interesting study used the host−guest methodology to synthesize a dual-metal-site $Fe_1Co_1$/N-C catalyst (*41*). Here, the aforementioned Zn/Co BMOF was used as a host for encapsulation by the double-solvent method, and separation of the $FeCl_3$ precursor by molecular-scale cages of ZIF was followed by pyrolysis to remove ligands and form nitrogen-doped porous carbon (NPC) for stabilization of the cluster. Subsequently, a spatial isolation method was reported for the fabrication of highly stable ISA Fe/NPC materials by a cage encapsulated-precursor and pyrolysis strategy (*42*). During the synthesis, iron(III) acetylacetonate was encapsulated and became trapped within the cages of ZIF-8. This resulted in suppression of the migration of Fe precursors, as the pore diameter of ZIF-8 is much smaller than the molecular diameter of iron(III) acetylacetonate. Thus, the successful confinement and spatial isolation of the active centers using an MOF as an isolator enabled the formation of Fe ISAs. This strategy can be expanded by replacing the host, as in the variously reported synthesis of series of $M_1$/N-C materials by ZIF-8-derived strategies (*43*, *44*). These researchers also developed a ZIF-assisted strategy for the fabrication of atomically dispersed single Ni atoms on the NPC through a synthesis based on ion exchange between Zn nodes and adsorbed Ni ions within ZIF-8 cavities followed by pyrolysis at 1000 °C (*45*). Yang et al. (*46*) reported the transformation of Ni NPs into Ni single atoms on the pyrolysis-treated ZIF-8 surface

through a thermal diffusion mechanism. Here, the researchers proposed that Ni NPs could break C–C bonds, leaving abundant pores, and diffuse into the N-defective carbon matrix. Exposure of Ni NPs to N-rich defects results in strong coordination, leading to the atomization of the Ni NPs. In addition to non-noble metals, Ji et al. (*47*) reported that single Ru atoms could be synthesized on MOF-derived supports through the encapsulation of $Ru_3(CO)_{12}$ in molecular-scale cages of ZIFs followed by pyrolysis at 800 °C. In another work, Li and co-workers (*48*) reported the conversion of palladium particles embedded in N-C derived from ZIF-8 into single atoms at 900 °C under an inert atmosphere for 3 h. From scanning transmission electron microscopy (STEM), morphological studies of the nanocomposite were recorded at different heating stages. It was observed that, initially, the Pd NPs grew larger in size, but subsequent heating led to continuous collisions and coordination of surface Pd with N-C to form single atoms. Zhang et al. (*49*) also reported a unique spatial isolation method for fabricating well-dispersed single Fe atoms on hierarchically structured porous carbon as the carbon support. They took advantage of the π−π stacking within unsubstituted phthalocyanine/iron phthalocyanine complexes to prevent the agglomeration of Fe species under high-temperature pyrolysis conditions. Jiang and co-workers (*50*) used a porphyrinic MOF as the precursor based on a mixed-ligand strategy to prepare high-loading single-atom Fe-implanted NPC by pyrolysis. Zhang et al. (*51*) reported a core–shell strategy for synthesizing single metal atoms anchored on N-C materials. This synthetic strategy included coating FeOOH nanorods with polymers such as polydopamine, followed by high-temperature pyrolysis resulting in carbonization of the polymer shell. In this process, the polydopamine layers were converted into a N-C shell, whereas the α-FeOOH was reduced to Fe with strong interactions between the Fe and the N-C shell to form Fe ISAs. The unstable ferric oxides in the core after pyrolysis were removed by acid etching to obtain homogeneous $Fe_1$/N-C. This method can be readily expanded by replacing the core FeOOH with $Co(OH)_2$, $Ni(OH)_2$, and $MnO_2$ for the fabrication of $Co_1$/N-C, $Ni_1$/N-C, and $Mn_1$/N-C, respectively. Chen et al. (*52*) developed a combined polymer and MOF confined pyrolysis strategy to construct a functionalized nanostructured composite with a hollow interior by the Kirkendall effect. Here, simultaneous electronic modulation of the Fe−$N_x$ center (where $x = 4$) was achieved through the long-range interaction of sulfur and phosphorus. A material with iron ISAs supported on nitrogen, phosphorus, and sulfur codoped hollow carbon was synthesized and was found to exhibit superior performance in the oxygen reduction reaction in alkaline media. Chen et al. (*53*) also developed a tungsten single-atom catalyst anchored on MOF-derived N-C following a pyrolysis strategy. Here, uncoordinated amine groups prevented the agglomeration of W species. Wang et al. (*54*) reported a coordination-based strategy for the precise control of single ruthenium atoms supported on an MOF (UiO-66). This synthesis was based on the utilization of strong interactions between uncoordinated $–NH_2$ groups and $Ru^{3+}$ ions to immobilize Ru. Thus, atomically disperse single Ru sites remain confined in the pores of the MOF without aggregation during high-temperature pyrolysis. The mechanism of formation is shown in Figure 5.

Qu et al. (*55*) developed a gas-migration strategy to access single-atom catalysts (SACs) of Cu, Co, and Ni in which no premixing of the metal precursor with the MOF was needed. This strategy was based on direct thermal emission from the bulk metals and the trapping of metal atoms by defects of MOF-derived nitrogen-rich carbon with the facilitation of $NH_3$. This gas-migration strategy avoids complex operating steps and is easy to scale up, being capable of producing different atomic metals in a more scalable manner compared to the conventional method. With a similar strategy, Sun and co-workers (*56*) demonstrated a simple metal–organic gaseous doping approach

to generate high-density single Fe atoms embedded in a ZIF-derived doped-carbon support by the thermal emission method. In this strategy, an iron compound, namely, evaporable ferrocene (sublimed above 100 °C), was first vaporized and then trapped into ZIF-8 precursors, which were subsequently pyrolyzed. At a pyrolysis temperature of 950 °C, the ZIF-8 was transformed into a porous carbon nanoframe, and the adsorbed ferrocene was transformed into a single Fe atom coordinated with N on the carbon skeleton.

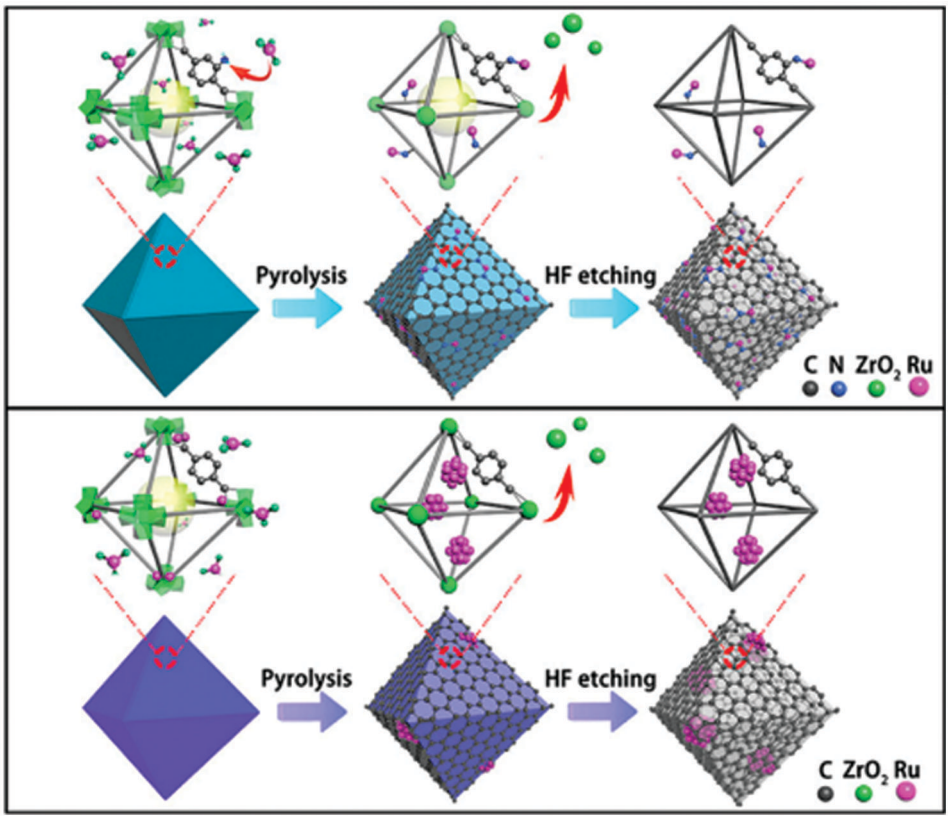


*Figure 5. Scheme of the proposed formation mechanisms for Ru SAs/N-C (top) and Ru NCs/C (bottom). Reproduced with permission from reference* (*54*). *Copyright 2017 American Chemical Society.*

### *2.1.4. Microwave-Assisted Method*

Microwave- (MW-) assisted synthesis is a bottom-up approach that is well-known for its sustainable, environmentally benign, and energy-efficient nature in synthesizing various NCs (*57*–*59*). MW synthesis is generally used for particle size reduction and dissolution enhancement. In comparison to other conventional heating methods, which involve conductive and convective heat transfer, the MW method provides homogeneous heating by reducing the effects of thermal gradients in the reactant solution. Therefore, MW methods favor the rapid homogenous nucleation and shorter crystallization time of NCs to yield high-purity monodisperse NPs with average diameters in the range of 1–2 nm and various shapes (*60*, *61*). Size-selected metal NCs of high purity and stability can be fabricated without further complex protective agents. This rapid synthesis method allows much time-consuming organic synthesis to occur within a few minutes (*62*). Liu et al. reported the synthesis of highly fluorescent Ag NCs in aqueous solution by a rapid MW-assisted method within 70 s; they obtained highly monodisperse and stable NCs with an average size 2 nm (*63*). Another

interesting study was reported by Kawasaki et al. (*64*), who demonstrated a MW polyol method for the synthesis of stable, highly blue fluorescent Cu NCs without the addition of any protective or reducing reagents. Fei et al. reported a convenient, ultrafast, and generalized MW synthesis protocol for the fabrication of atomic Co/Ni/Cu metal embedded nitrogen-doped graphene (*65*). MW heating of the reactant mixture of amine-functionalized graphene oxide (GO) and the corresponding metal precursors provided, within 2 s, highly monodisperse graphene-supported single atomic transition metals, as shown in Figure 6.

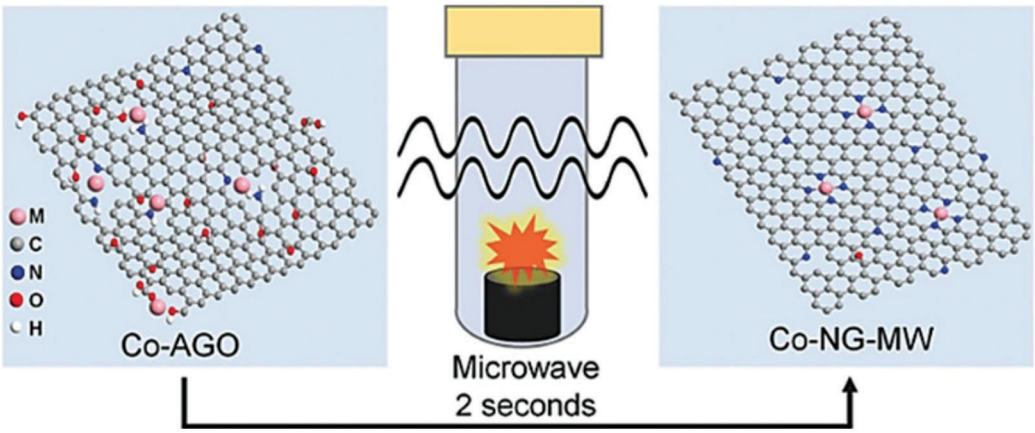


*Figure 6. Schematic illustration of the preparation of graphene-supported Co atoms by a MW-assisted synthesis route. Abbreviations: AGO, amine-functionalized graphene oxide; NG, nitrogen-doped graphene. Reproduced with permission from reference* (*65*). *Copyright 2018 Wiley-VCH.*

In this one-pot synthesis, MW heating induced a simultaneous reduction of GO to graphene and nitrogen-doped graphene and the effective incorporation of the transition-metal atoms into the graphene lattices. This reduced the metal aggregation and established a unique single-metal-atom dispersion on graphene.

### *2.1.5. Photochemical Reduction*

Photochemical reduction, which includes the absorption of photons and the creation of electronically excited states, is a bottom-up technique and an effective tool for synthesizing NPs of precise sizes (*66*). This synthesis methodology received significant consideration from the scientific community after a report on the size-dependent fluorescence studies of Ag NCs by Peyser et al. (*67*) Zheng and co-workers developed a room-temperature photochemical solid-phase reduction method for fabricating a stable and highly concentrated $Pd/TiO_2$ (1.5 wt %) material (*68*). First, the Pd species were adsorbed on a support of two-atom-thick $TiO_2$ nanosheets modified with ethylene glycolate. The obtained $H_2PdCl_4/TiO_2$ material was irradiated under UV light, which induced ethylene glycolate radicals to remove $Cl^-$ ligands and form Pd single atoms (*69*). The highly stable $Pd/TiO_2$ catalyst exhibited high catalytic activity in hydrogenation of benzaldehyde. The Luo group synthesized single Pt atoms embedded in nanosized anatase $TiO_2$ present in (101) facets (*70*). Wei et al. (*71*) developed an ultralow-temperature photochemical reaction method in which chloroplatinic acid with an antifreeze solution (ethyl alcohol and water) was irradiated with UV light at −60 °C. Atomically dispersed Pt metal with a size of 0.1 nm adsorbed in N-doped mesoporous carbon was effectively prepared. Wang's group reported a photochemical solid-phase reduction route for the

synthesis of distinct isolated Pt atoms with a narrow size range (<0.4 nm) anchored on NPC (*72*). In this synthesis, $PtCl_6^{2-}$ ions were reduced by UV light and then adsorbed on highly porous abundant defect sites on the NPC surface without physical or chemical post-treatment. A schematic of this synthesis method is shown in Figure 7.

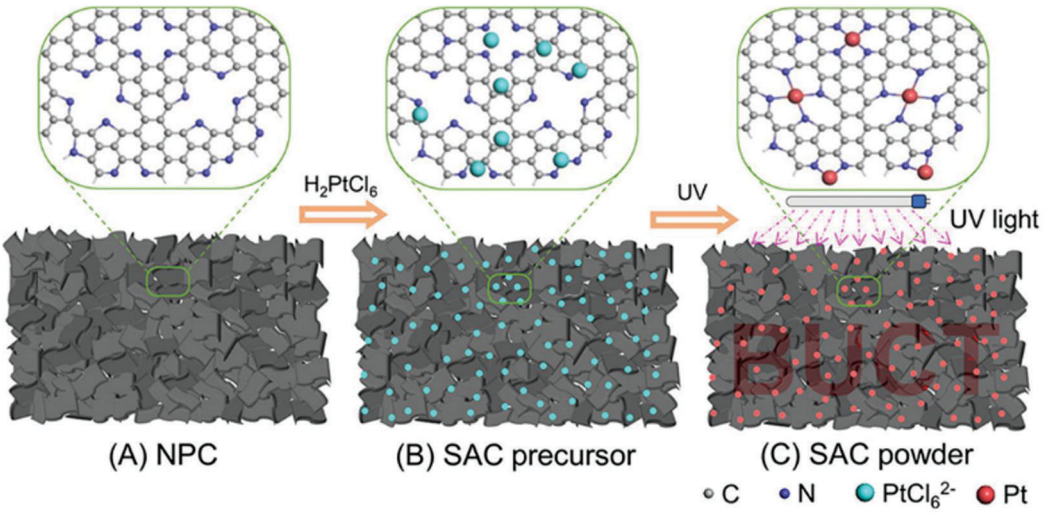


*Figure 7. Schematic illustration of the formation of $Pt_1$/NPC catalyst: (A) NPC substrate, (B) $PtCl_6^{2-}$ ions adsorbed on the NPC, and (C) Pt single atoms anchored on the NPC. Reproduced with permission from reference* (*72*). *Copyright 2018 American Chemical Society.*

The synthesized Pt-based catalyst showed good stability and outstanding electrocatalytic activity for the oxygen reduction reaction and the hydrogen evolution reaction (HER). Considering the UV-limited reducing capacity, the applicability of this approach for non-noble metal atoms is still questionable (*66*).

Considering that the aggregation of metal atoms and NCs can be suppressed at low temperatures, Wu and co-workers (*73*) demonstrated iced photochemical reduction using the UV irradiation of a frozen chloroplatinic acid solution to generate atomically dispersed platinum atoms. The single platinum atoms were deposited on various substrates, such as mesoporous carbon (MC), multiwalled carbon nanotubes, graphene, $TiO_2$ NPs, and ZnO nanowires. Of these, $Pt_1$/MC exhibited significant stability for the electrochemical HER reaction. The HER activity and catalyst stability of $Pt_1$/MC could be attributed to the unique electronic properties of Pt/MC and the stronger Pt–MC substrate interaction, respectively, compared to other conventional Pt surfaces. Photochemical reduction under iced conditions prevented the aggregation of atoms and other stable single atoms; for example, gold and silver were also obtained.

### *2.1.6. Atomic Layer Deposition*

Another effective method for obtaining subnanometer-scale catalysts with high atomic precision is atomic layer deposition (ALD). This technique can be categorized as bottom-up fabrication. In the ALD process, a substrate is exposed to vapors of different reactive precursors. A surface self-limiting reaction occurs between the precursor and functional groups on the substrate. The reaction continues until all of the available surface functional groups are consumed. Purging with inert gas is

used to remove any volatile byproducts and unreacted precursor. This step is followed by reaction with the next precursor. ALD is typically a thin-film growth technique that is a subset of chemical vapor deposition and depends on self-limiting binary reactions between gaseous reactant molecules and a suitable substrate to deposit a uniform film in a layer-by-layer fashion (*74–76*). Lu and Stair (*77*) reported a novel ALD method for synthesizing highly uniform ultrafine supported Pd metal NPs with sizes in the range of 0.3–2.5 nm that included growing the protected metal NPs and new support layers at the relatively low temperature of ~150 °C. A detailed schematic model of the ALD process is provided in Figure 8.

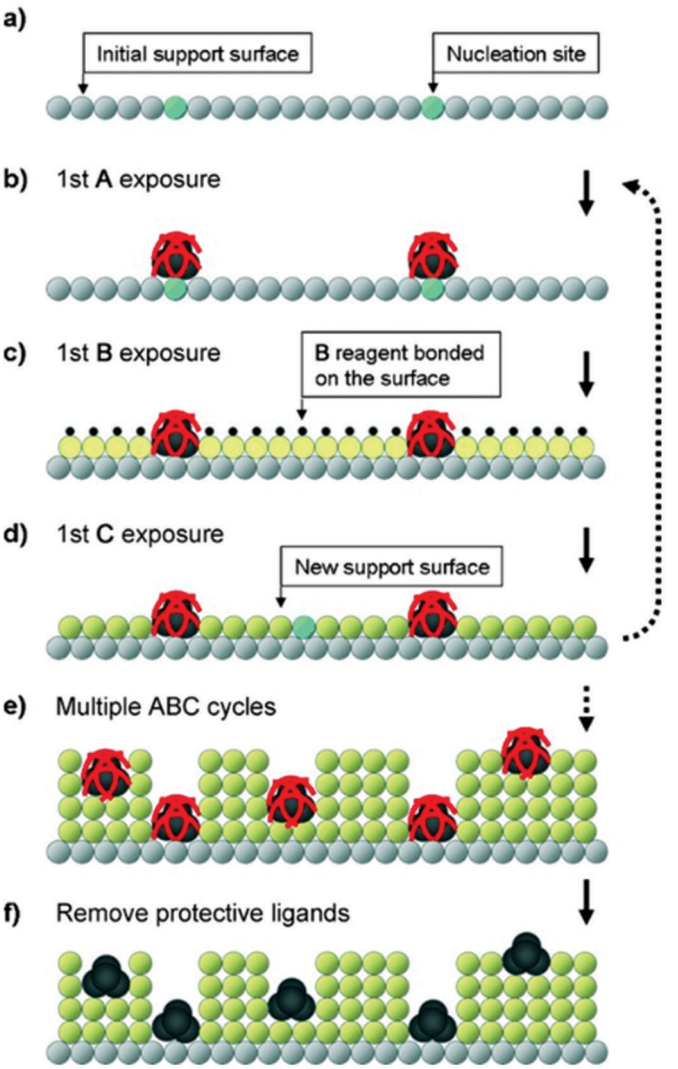


*Figure 8. Schematic model of ABC-type ALD: (a) Initial support with nucleation sites. (b) Introduction of volatile metal precursor A onto the surface to form metal NPs with part of the retained ligands (red curves). (c) Introduction of the first reagent B onto the surface. (d) Introduction of the second reagent C onto the surface to react with B and form a new support surface. (e) New support and metal NPs protected by ligands formed on the initial support surface after multiple ABC cycles. (f) Removal of the protective ligands to activate the metal NPs. Reproduced with permission from reference* (*77*)*. Copyright 2010 Wiley-VCH.*

Botton and co-workers (*78*) reported the synthesis of a mixture of isolated Pt atoms and Pt NCs on a N-doped graphene surface using the ALD technique. Later, various reports on the synthesis of bimetallic NP catalysts by the ALD method with precise control over both the particle size and composition were published in the literature. Through control of the number and order of executed cycles, the preferred sizes and structures of bimetallic catalysts were achieved. One developed procedure can be applied as a generalized approach for the preparation of a variety of bimetallic catalysts on any substrate at any quantity. Sun et al. (*79*) reported a practical synthesis of Pt ISAs, SNCs, and NPs with average sizes of 0.5, 1–2, and 2–4 nm, respectively, corresponding to 50, 100, and 100 cycles of uniform deposition on graphene using the ALD technique. Their study revealed that the morphology, size, density, and loading of Pt on the graphene surface could be accurately controlled by merely adjusting the number of ALD cycles. Yan et al. (*80*) successfully established the ALD of atomically dispersed Pd on graphene by carefully controlling the oxygen functional groups on the graphene surface. Owing to issues of scalability and high cost, commercial catalyst preparation using this method is limited (*81*).

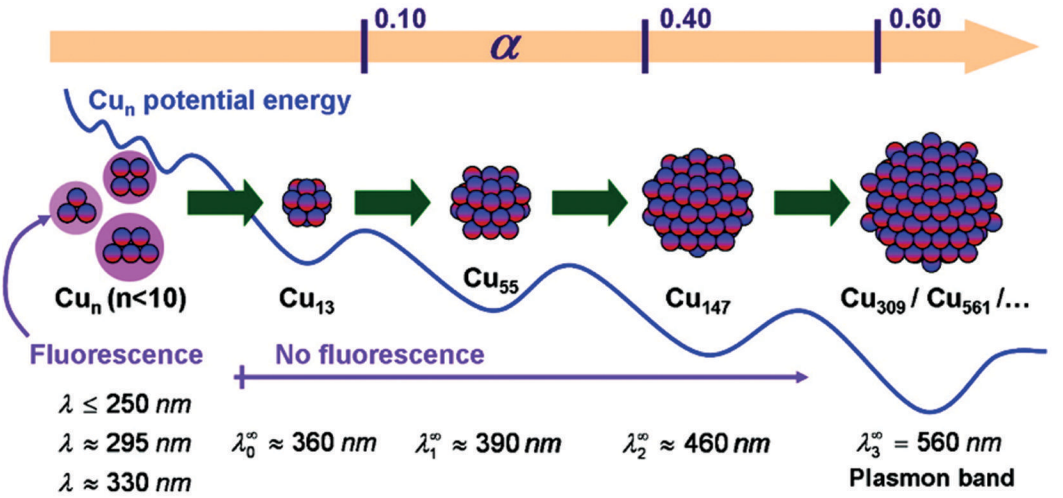


*Figure 9. Schematic of the evolution of the copper cluster size with increasing α value. Reproduced with permission from reference (87). Copyright 2009 American Chemical Society.*

### *2.1.7. Microemulsion Technique*

The microemulsion technique is a very flexible bottom-up synthesis approach that has great potential in the fabrication of a variety of atomic, subnanoscale structures alone or in combination with other techniques. It has many possibilities for applications to atomic, subnanoscale structures, with the only limitation being researchers' imagination (*82*). Microemulsions are transparent, isotropic, and thermodynamically stable colloidal nanodispersions of water and oil ( water-in-oil or oil-in-water) stabilized by a surfactant film. The surfactant-covered water pools can form a distinct liquid core–shell structure at the subnanoscale level and, thus, can act as nanoreactors for the performance of many chemical reactions, in particular the synthesis of nanomaterials (*83*). The method involves the mixing of two microemulsions or of a microemulsion and an aqueous solution containing the appropriate reactants to obtain NPs with diameters in the range between 5 and 50 nm (*84*). Through careful control of the reaction parameters, these nanoreactors can yield subnanometer custom-made products with predesigned properties. For example, this method was successfully

employed to synthesize a series of atomic copper clusters with different core sizes. Specifically, Qiu et al. (*85*) synthesized spherical Cu NPs in sodium dodecyl sulfate/isopentanol/cyclohexane/water microemulsions using sodium borohydride as a reducing agent. The diameters of the Cu NPs increased with increasing mole ratio of water to surfactant and concentration of $Cu^{2+}$ solution within the size range of 2.75–39 nm for water-to-surfactant mole ratios of 5–30 at a $Cu^{2+}$ concentration of 0.1250 M and within the size range of 9.8–39.4 nm for $Cu^{2+}$ concentrations of 0.1250–0.500 M at a water-to-surfactant mole ratio of 10. Another interesting study on the synthesis of stable $Ag_n$ clusters ($n \leq 10$) by kinetic control has also been reported (*86*). Later, Rivas and co-workers modified and reported a successful synthesis of small atomic copper clusters ($Cu_n$) by precise control of the size through fine-tuning of the amount of reducing agent used in the reaction mixture (*87*). A schematic illustration of the evolution the Cu cluster size is shown in Figure 9. One of the disadvantages of this technique is the high consumption of organic solvents during the synthesis of certain magnetic NPs (*88*).

### *2.1.8. Dimethylformamide-Based Reduction Methods*

Dimethylformamide- (DMF-) based reduction methods are bottom-up techniques. This type of chemical reduction method, which is frequently used for the synthesis of subnanometer NPs, often employs some protecting ligands to stabilize the tiny metal cores, and this results in the incomplete reduction of the metal atoms. However, the use of DMF has been demonstrated to be a viable solution to this problem. DMF can serve three roles in the synthesis of NPs, namely, as a solvent, as a reductant, and also as a protectant, as shown in Figure 10.

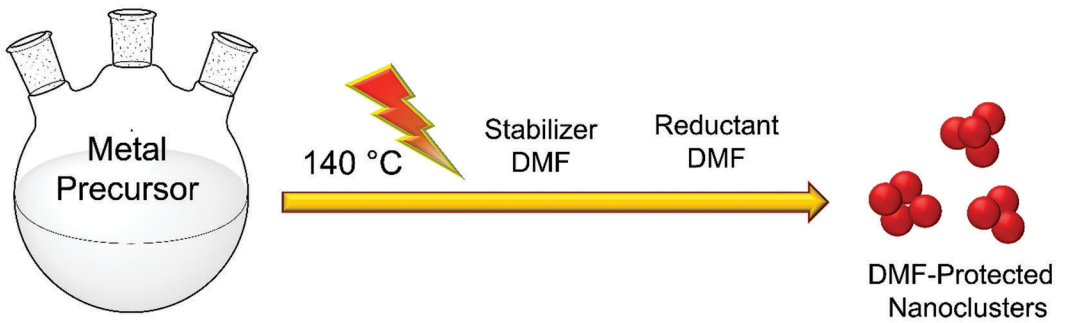


*Figure 10. Synthesis of metal NCs by the DMF-based reduction method.*

Liu et al. prepared fluorescent Ag NCs by using DMF as a solvent as well as the reducing agent (*63*). The resultant surfactant-free Ag NCs were found to exhibit bright fluorescence, and their optical behavior could be easily tuned by additional functionalization and the use of capping molecules. Later, Kawasaki et al. (*89*) modified the latter method and demonstrated the synthesis of highly stable fluorescent DMF-protected Au NCs by a surfactant-free DMF reduction method. The synthesis proceeded without the formation of gold NPs and any bulk metals as the byproducts. The obtained Au NCs were a combination of various-sized Au NCs with fewer than 20 atoms per cluster and core diameters of less than 2 nm, including at least $Au_8$ and $Au_{13}$. Further, the method has been applied to the surfactant-free solution synthesis of fluorescent Pt NCs comprising four to six Pt atoms (*90*). The obtained Pt NCs were very stable and readily dispersible in organic, aqueous, and salt solutions. This synthesis approach has also been applied successfully to other platinum-group metals (*91*).

*2.1.9. Radiolytic Approach*

The radiolytic approach to synthesis is based on the interaction of matter with high-energy ionizing radiation (*92*). Here, γ-rays are used to produce solvated electrons from an aqueous solution. These solvated electrons further reduce the metal ions to metallic clusters. With this method, the size of the metal NPs can be effectively controlled by changing the stabilizer, radiation source, precursor concentration, and so on. This method uses no harsh reducing agents, and the reaction occurs in an aqueous environment at ambient conditions. The large-scale synthesis of NCs is the main advantage of this technique. Figure 11 explains the basic mechanism and the elementary processes leading to the formation of metal and alloy NPs by this method.

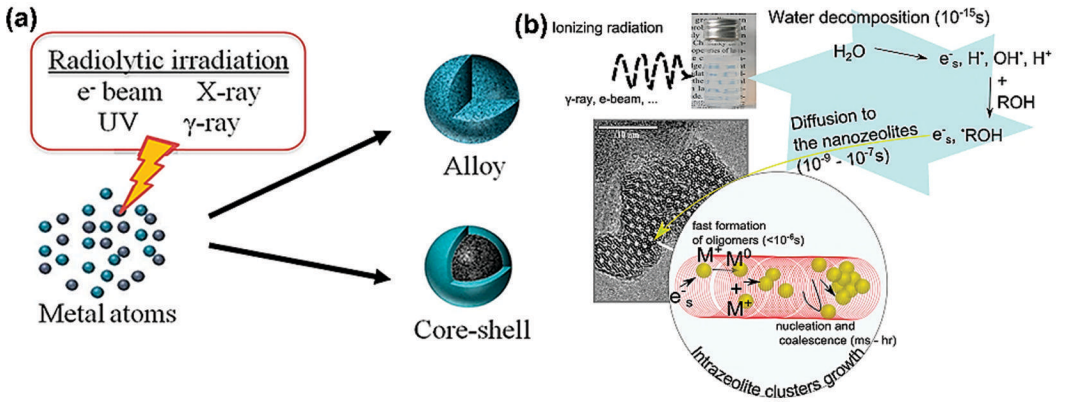


*Figure 11. (a) Synthesis of alloy and core–shell NPs using the radiolysis approach. (b) Elementary processes and time scales governing the formation of metal and alloy NPs in colloidal suspensions of zeolite nanocrystals. Reproduced with permission from reference* (*93*)*. Copyright 2018 American Chemical Society.*

Ag NCs containing several atoms have been prepared in the presence of polyphosphate or polyacrylate in aqueous solution with simple γ-ray irradiation (*94*, *95*). Specifically, an aqueous solution containing the silver salt ($AgClO_4$) and the polymer (sodium polyphosphate or sodium polyacrylate) was exposed to γ-ray irradiation. The solution also contained an alcohol, such as methanol, *tert*-butyl alcohol, or 2-propanol, to scavenge the OH– radicals generated during the radiolysis. Aggregation of NCs was a serious problem related to this synthesis. However, stabilizer-free radiolysis of Ag NCs from deaerated aqueous $AgClO_4$ solutions containing 0.2 M methanol were also reported (*96*). The γ-ray irradiation created reducing species in the solutions, including hydrated electrons, H atoms, and $CH_2OH$ radicals. The main drawback of this process is the inability to capture the short-lived NCs, which limits the broad applicability of the synthesis.

*2.1.10. Electrochemical Synthesis*

This method is a frequently used bottom-up technique for preparing NCs. In this process, a two-electrode system is used to produce size-selected NCs of high purity. This method is flexible in nature; reaction parameters such as the electrolytic concentration can be used to directly modify the particle size. The introduction of the electrochemical reduction process to the preparation of subnanometric metals was first proposed by Reetz and Helbig (*97*), who synthesized Pd NPs with sizes of 1–5 nm by varying the reaction parameters. In this process, surfactants are added to an

electrolyte solution, a sacrificial anode serves as the metal source, and the metal ions produced are reduced at the cathode. The main merits of this method are its low reaction temperature; high yields; low costs; and easy tuning of NCs by controlling parameters such as the concentrations of the electrolyte and stabilizing agent and the current and voltage used. Intriguingly, the synthesis of fluorescent atomic Cu clusters with up to 14 atoms was achieved by a simple electrochemical process in which tetrabutylammonium nitrate was used as the stabilizer (*98*). This method is easy to scale up for the mass production of Cu clusters. By varying the current density of electrochemical procedure, López-Quintela and co-workers synthesized Ag NPs with sizes ranging from 2 to 7 nm (*99*). Rodríguez-Vázquez et al. (*100*) reported the synthesis of small atomic $Au_n$ clusters with $n \leq 11$ atoms through the anodic dissolution of a Au electrode using tetrabutylammonium bromide as the stabilizer and acetonitrile as the solvent. A recent report on the single-step electrochemical synthesis of Co NCs embedded on dense graphite sheets was reported by Renjith and Lakshminarayanan. (*101*). The method of electrodeposition provided a facile one-step route for the preparation of thin NCs of cobalt under ambient-temperature conditions, as shown in Figure 12.

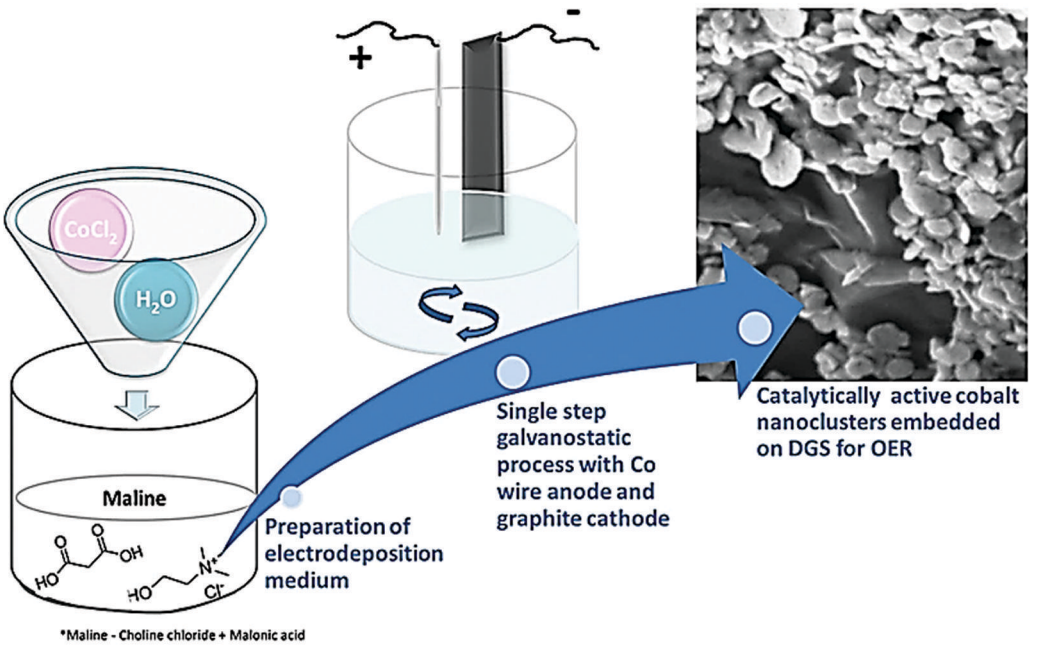


*Figure 12. Schematic illustration of the electrodeposition of Co NCs onto a graphite sheet. Abbreviations: DGS, dense graphite sheet; OER, oxygen evolution reaction. Reproduced with permission from reference* (*101*). *Copyright 2020 American Chemical Society.*

### *2.1.11. Template-Based Synthesis Methods*

Template-based syntheses have been successfully applied for the preparation of highly fluorescent subnanometer-sized metals. Generally, polymer, dendrimer, polyelectrolyte, protein, and DNA templates have been used to prepare metal NCs of various configurations with preferred morphologies and sizes. The uniqueness of this method is its ability to deliver a preset environment for the formation of NCs with precise sizes and shapes. This synthesis methodology received much scientific attention after a 1998 report on the preparation of stable Cu NCs using poly(amidoamine) (PAMAM) dendrimer templates (*102*). Cu NCs ranging in size from 4 to 64 atoms were prepared by

partitioning of $Cu^{2+}$ ions into the interior of a PAMAM Starburst dendrimer and then performing a chemical reduction. After the chemical reduction step, $Cu^{2+}$-loaded fourth-generation dendrimers with an ethylenediamine core resulted in the formation of Cu NCs with diameters of less than 2 nm. The cluster size could be controlled by changing the size of the PAMAM dendrimer, which also served the role of a stabilizer for the NCs. This methodology is applicable to the preparation of other transition-metal NCs as well. A dendrimer of polydentate ligands collects metal ions or salts into its interior, permitting the formation of metal NPs. The dendrimer-encapsulated NPs exhibit distinctive catalytic activities because of their size (*103*). The synthesis of a PAMAM dendrimer–Cu metal nanocomposite was reported later the same year by Balogh and Tomalia (*104*). The core–shell structure of the dendrimers is responsible for yielding and stabilizing the metal NCs. The internal core structure of the dendrimer, which contains tertiary amines, can make coordination bonds with the metallic ions, and the external shell can inhibit the aggregation of the as-synthesized clusters. Further, Zheng and Dickson (*105*) fabricated stable, fluorescent Ag NCs with single nanodots ranging in size from two to eight Ag atoms, within PAMAM dendrimer hosts in aqueous solutions. In another report, Ag NCs were prepared using DNA templates by making use of the high affinity of $Ag^+$ for DNA bases (*106*). Very small oligonucleotide-encapsulated Ag NCs were formed without the formation of large NPs by cooling the solution of DNA and $Ag^+$ to 0 °C and then adding $NaBH_4$ with vigorous shaking. Xie et al. (*107*) reported a simple, one-pot, green synthetic route for the synthesis of Au NCs ($Au_{25}$) at relatively low temperature (37 °C) using commonly available bovine serum albumin (BSA) protein. Upon the addition of Au(III) ions to the aqueous BSA solution, the protein molecules sequestered and entrapped the Au ions. In situ reduction of Au ions in the presence of BSA occurred at pH ~12 to form Au NCs.

Kumacheva's (*108*) group reported the successful synthesis of fluorescent Ag NCs through photoreduction by employing hydrogel-microsphere (polymer-microgel) templates. In the microgels, the concentrated carboxyl groups of the poly(acrylic acid) (PAA) moiety were critical for the immobilization of Ag ions and the formation of stable Ag NCs. The same group also reported the template-based synthesis of NPs, including metal, semiconductor, and magnetic NPs, in the interiors of PAA (*109*). They demonstrated that NPs with predetermined properties could be synthesized by tuning the reaction conditions, composition, structure, and NP concentration of the polymer microgels. The NP polydispersity was reduced by the heat post-treatment of hybrid microgels, resulting in controlled photoluminescence. Frey and co-workers (*110*) synthesized water-soluble fluorescent Ag NCs by using star-shaped polyglycerol-*block*-poly(acrylic acid) (PG-*b*-PAA) polymers as templates. The multiarm PG-*b*-PAA polymers were synthesized using atom-transfer radical polymerization. These polymers had a core–shell structure in which the local density of carboxyl groups decreased gradually from the core to the shell, resulting in a "cage effect". This effectively inhibited the formation of larger NPs, hence providing stability to metal NCs in the same way as "molecular hydrogel". Further taking advantage of the cage effect, Wei's group (*111*) reported the starlike polymers polyacrylate-*graft*-poly(acrylic acid) formed by the combination of atom-transfer radical polymerization and "click chemistry". These polymers were used as templates for the synthesis of silver NCs with UV light as a mild reductant. Meanwhile, Tan's (*112*) group employed a facile chain-transfer radical polymerization method to prepare three polymer ligands containing pentaerythritol tetrakis(3-mercaptopropionate) with poly(methyl methacrylate), poly(*n*-butyl methacrylate), and poly(*tert*-butyl methacrylate). These polymer ligands were used to synthesize blue Au NCs by a photoreduction method. These polymer ligands have amplified electron-donating abilities compared to their monomer counterparts and promote fluorescence in

the resulting Au NCs. In another work, Gao's group (*113*) designed gold NPs coated with thiol polystyrene macromolecules uniformly dispersed in a polystyrene matrix. This generated the core–shell-structured hyperstar polymer through atom-transfer radical copolymerization of an inimer with disulfide groups. These hyperstar polymers efficiently encapsulated presynthesized $Au_{25}(SR)_{18}$ NCs through ligand exchange to give highly stable $Au_{25}(SR)_{18}$ nanocomposites. The obtained Au nanocomposites showed a highly efficient catalytic reduction reaction of 4-nitrophenol. Lennox and co-workers (*114*) demonstrated that blending of polymer-ligand-stabilized gold NPs into a presynthesized polymer can generate stable nanocomposites in situ. The principal advantage of this method resides in the full synthetic control it provides over both the NPs and the polymer matrix. Figure 13 shows the application of different template-assisted syntheses of metal NCs.

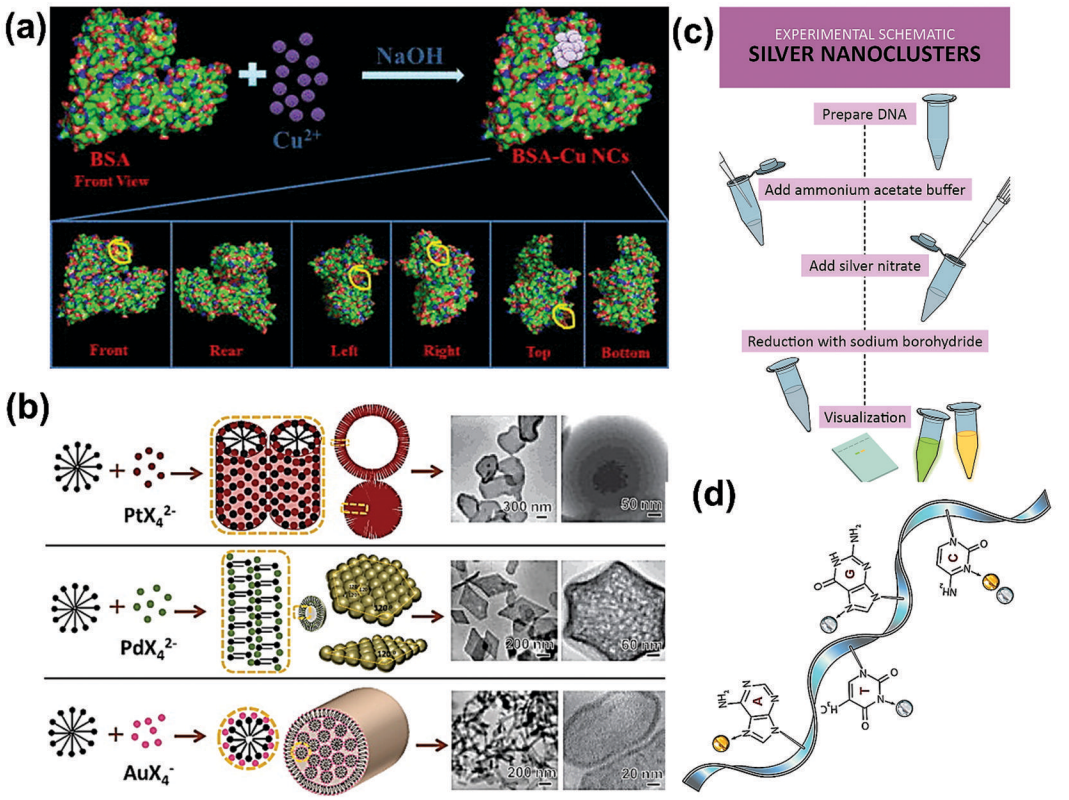


*Figure 13. (a) Schematic illustration of the step-by-step formation of Ag NCs using DNA templates. Reproduced with permission from reference* (*117*). *Copyright 2020 American Chemical Society. (b) Proposed primary metal coordination sites of DNA to gold and silver atoms. Reproduced with permission from reference* (*118*). *Copyright 2018 American Chemical Society. (c) Synthesis of noble-metal NCs with variable micellar templates. Reproduced with permission from reference* (*116*). *Copyright 2014 American Chemical Society. (d) Schematic of the formation of Cu NCs on the BSA surface. Reproduced with permission from reference* (*115*). *Copyright 2014 AIP Publishing.*

### *2.1.12. Wet-Chemical Route*

The wet-chemical synthesis route is a very simple bottom-up method for the large-scale preparation of nanocatalysts. The common wet-chemical route involves impregnation and coprecipitation. In wet-chemical routes for the preparation of SACs, the precursor materials are

dispersed on suitable supports by means of a chemical reaction. The supports used should be capable of offering enough anchoring sites for the metal atoms to prevent aggregation through metal–support interactions (*69*). Qiao et al. (*119*) reported the synthesis of Pt ISAs anchored to the surfaces of iron oxide nanocrystallite ($Pt_1/FeO_x$) catalysts (where $x$ is the coordination number) by the coprecipitation method followed by a post-treatment procedure. Afterward, a systematic study of the synthesis by the coprecipitation method of a series of $Ir/FeO_x$ catalysts with different Ir loadings was reported (*120*). Precipitation temperatures as low as 80 °C were used to confirm the complete precipitation of $H_2IrCl_6$ in the solution followed by complete loading onto the $FeO_x$ support. In addition, bimetallic uniformly distributed core–shell PtPd@Pt nanocrystals supported on reduced graphene oxide (rGO) were successfully synthesized by a facile and green wet-chemical procedure (*121*). Figure 14 illustrates the synthesis mechanism of PtPd@Pt nanocrystals on rGO.

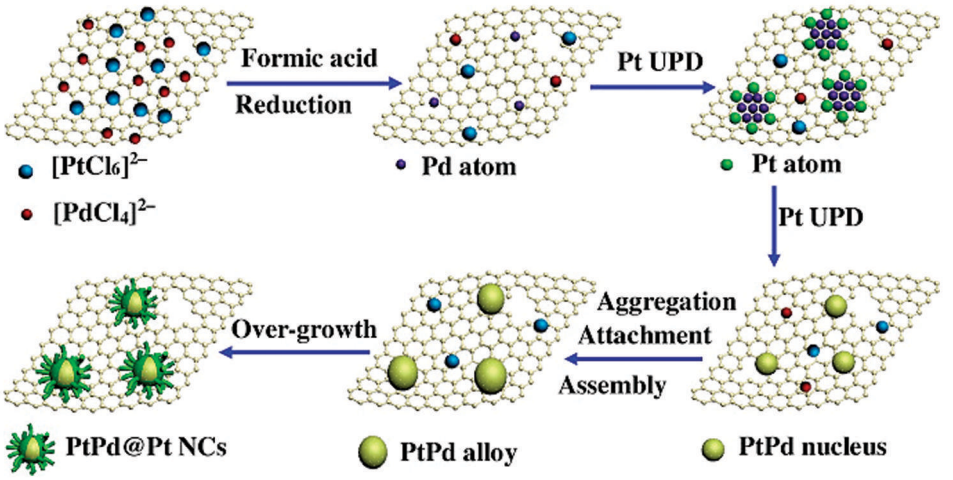


*Figure 14. Formation mechanism of bimetallic core–shell PtPd@Pt NCs supported on reduced graphene oxide (PtPd@Pt NCs/rGO). Abbreviation: UPD, underpotential deposition. Reproduced with permission from reference* (*121*). *Copyright 2016 Elsevier.*

Initially, $[PdCl_4]^{2-}$ was reduced by Pt atoms formed on the metallic Pd surface by underpotential deposition. Subsequently, Pd atoms were produced by reduction of $[PdCl_4]^{2-}$ with formic acid. During the process, the Pd atoms covered the Pt surface, and the Pd atoms occupied the Pt sites, thereby removing Pt atoms from the crystal lattice. Formic acid induced the formation of PtPd nuclei, which resulted in the formation of PtPd alloy NPs through surface attachment, self-aggregation, and assembly. The remaining $[PtCl_6]^{2-}$ was successively reduced to Pt atoms and further deposited on the surface of the PtPd alloy, finally resulting in the formation of core–shell PtPd@Pt NCs on rGO through the overgrowth process. In this case, formic acid was used as the reducing agent without the use of any additive such as a surfactant, polymer, seed, or template. Hackett et al. reported the synthesis of $Pd/Al_2O_3$ catalysts with Pd loadings between 0.03 and 4.70 wt % by a wet-impregnation method (*122*). Zhang et al. synthesized a series of $Au/ZrO_2$ catalysts with different metal loadings ranging from 0.01 to 0.76 wt % by a deposition–precipitation wet-chemical route (*123*). Another novel wet-chemical route is the galvanic replacement reaction used by Li et al. (*124*) to synthesize $Pt/MoS_2$ catalysts. In a typical synthesis method, $K_2PtCl_6$ solution

was injected into a mixture containing water, ethanol, and $MoS_2$ nanosheets by means of a syringe pump where the Mo atoms in the $MoS_2$ nanosheets were replaced by Pt. Another method involves the impregnation technique in which the active-metal-containing reaction precursor is mixed with a suitable catalyst support. The metal precursor is then allowed to anchor onto the support through ion exchange and adsorption. Many noble metals supported on graphene and graphitic carbon nitride have also been reported (*125*–*128*).

#### *2.1.13. Solid-State Route*

The solid-state route is a bottom-up technique for the synthesis of NCs in macroscopic quantities. The solid-state synthesis method is generally used to synthesize inorganic materials because of its advantages such as facile process, low-cost precursors, and large-scale synthesis of materials. This method allows control of the size, shape, and composition of NCs. Often, its application is limited because it requires extreme reaction conditions such as high temperatures or pressures. However, in the case of the gram-scale synthesis of metal NCs, this approach is highly preferred. In the solid-state process, individual reaction precursors are first mixed in stoichiometric quantities and then ground well to obtain a homogeneous mixture. This grinding can be performed by different methods such as mortar and pestle or ball milling. Annealing at elevated temperature is usually performed to obtain a compact and improved thermal reactive powder. Pradeep and coworkers reported the direct solid-state synthesis of subnanometer-sized $Ag_9$ quantum clusters consisting of a nine-atom core with mercaptosuccinic acid as a capping agent (*129*). In this method, all reaction precursors were present in the solid state, resulting in controlled particle growth and minimized diffusion of reactants. Gram quantities of highly stable NCs have been synthesized in the solid state under inert atmospheres. Haruta and co-workers synthesized gold clusters deposited on porous coordination polymers by a simple mortar grinding method (*130*). They found that Au clusters supported on Al-$MIL_{53}$ could catalyze the one-pot synthesis of secondary amines by sequential oxidation and hydrogenation of primary amines. The same clusters could promote the *N*-alkylation of aniline with benzyl alcohol to form the secondary amine under an inert atmosphere. Sakurai's group synthesized bimetallic gold–silver alloy NCs by a solid-state route (*131*). In this method, sequential reduction occurred by simple solid grinding, with chitosan as the reducing and stabilizing agent. These bimetallic clusters were found to exhibit good synergistic catalytic activity for the reduction of 4-nitrophenol as the model reaction. Liu et al. (*132*) reported a milling-based solid reduction technique for the preparation of ultrafine Au clusters. During the synthesis, solid grinding was followed by in situ reduction of gold precursors by $NaBH_4$ to give Au clusters on a Schiff base-functionalized silica support. This solvent-free method restrained crystal nucleation to facilitate the formation of a stable Au SNC. Deng and co-workers (*133*) demonstrated that the eggshell membrane could be employed as an efficient solid synthetic platform for the generation of fluorescent gold and silver NCs in monolithic form. These eggshell-membrane-based NCs displayed efficient control over nucleation and growth and have a wide range of applications as recyclable catalysts, surface-enhanced Raman scattering interfaces, fluorescent patterning materials, and anti-counterfeiting components.

### 2.2. Top-Down Approaches

In top-down approaches, the subnanometric particles and their clusters are synthesized from larger-sized particles by decreasing the size or by core etching. In this case, the NPs are prepared first and are then reacted with additional ligands or metal ions to form clusters. Gold NCs of $Au_8$

and $Au_{25}$ with luminescent properties have been synthesized by this approach. Duan and Nie used a polyethylenimine dendrimer to synthesize water-soluble, highly luminescent $Au_8$ NCs from dodecylamine-capped metal NPs by a ligand-induced etching process (*134*). Qian et al. (*135*) reported the synthesis of highly monodisperse $Au_{25}$ NCs from polydisperse Au NPs through a thiol etching process. In this case, Au NPs were prepared by the $NaBH_4$ reduction of a Au(III) salt in the presence of triphenylphosphine. The synthesized NPs were used for the syntheses of both $Au_{25}$ nanorods with a length of 1.1 nm and a diameter of 0.5 nm and $Au_{25}$ nanospheres (~1 nm in diameter), followed by thiol etching. A schematic illustration of the synthesis protocol is presented in Figure 15.

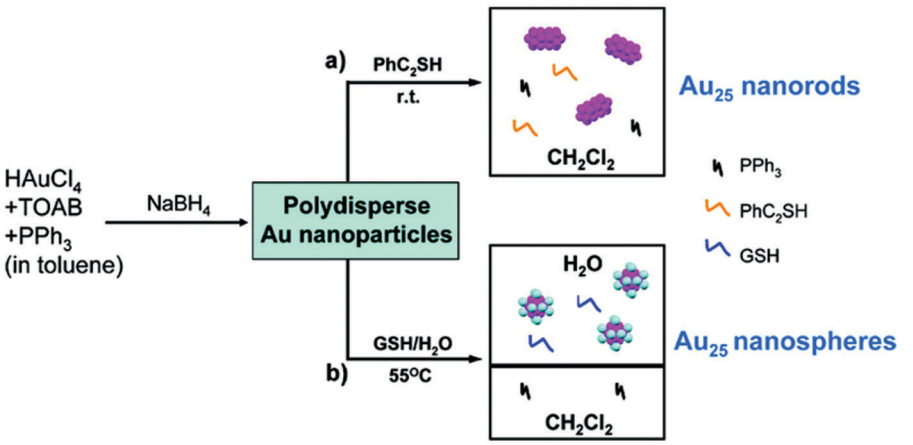


*Figure 15. Conversion of polydisperse Au NPs into atomically monodisperse $Au_{25}$ nanorods and nanospheres by (a) one-phase and (b) two-phase thiol etching. Abbreviations: GSH, glutathione; TOAB, tetraoctylammonium bromide. Reproduced with permission from reference* (*135*). *Copyright 2009 American Chemical Society.*

The size and shape of the NPs were effectively controlled by various thiol ligands in the second phase of the thiol etching process (*135*). Another report described the synthesis of water-soluble fluorescent gold NCs capped with dihydrolipoic acid, in which didodecyldimethylammonium bromide was used for the stabilization of the NPs (*136*).

### *2.2.1. Ligand-Exchange Method*

The ligand-exchange method is a top-down approach that generally consists of two steps: synthesis of the precursor and then the ligand exchange with the target functional ligand. The development of this method was based on the size-focusing process. A new ligand is added to a solution of metal NCs that are already protected by an initial ligand. The interaction between the two ligands results in the dynamic structural transformation of the original metal NCs, where the original ligands are replaced by the new ligand (*137*, *138*). NCs of gold, silver, and copper, as well as their alloys, have been successfully synthesized by this technique. In a typical synthesis, NCs are initially synthesized using a thiol route and subsequently etched by adding a different thiol in excess to the reaction mixture. This additionally added thiol often exhibits a larger steric hindrance than the originally added thiol, thereby resulting in a higher probability of NC formation. By using 4-*tert*-butylbenzenethiol (TBBT), the Jin group successfully prepared Au-based NCs such as

$Au_{28}(TBBT)_{20}$ (*139*), $Au_{36}(TBBT)_{24}$ (*140*), $Au_{20}(TBBT)_{16}$ (*141*), $Au_{133}(TBBT)_{52}$ (*142*), and $Au_{92}(TBBT)_{44}$ (*144*). The same group also used other thiol protecting groups to prepare additional NCs based on noble metals, including $Au_{24}(SCH_2Ph\text{-}^tBu)_{20}$ (where $SCH_2Ph\text{-}^tBu$ = 4-*tert*-butylphenylmethanethiolate) (*143*) and $[Pt_1Ag_{28}(S\text{-}Adm)_{18}(PPh_3)_4]^{2+}$ (where S-Adm = 1-adamantanethiolate) (*145*), and Xu et al. prepared the Au-based selenolate-protected NC $Au_{18}(SeC_6H_5)_{14}$ (*146*). Another significant study involved the thiol-ligand-induced transformation of $Au_{38}(SC_2H_4Ph)_{24}$ into $Au_{36}(TBBT)_{24}$ by Zeng et al. (*147*) They proposed a disproportionation mechanism for the conversion of rodlike biicosahedral $Au_{38}(SC_2H_4Ph)_{24}$ into tetrahedral $Au_{36}(TBBT)_{24}$ NCs. When the ligand exchange of $Au_{38}(SC_2H_4Ph)_{24}$ is done with the bulkier TBBT, the latter causes structural collapse of the initially formed $Au_{38}(SC_2H_4Ph)_{24}$ structure, which releases two Au atoms and transforms into the $Au_{36}(TBBT)_{24}$ structure. The released Au atoms combine with $Au_{38}(SC_2H_4Ph)_{24}$, ultimately forming $Au_{40}(SC_2H_4Ph)_{26}$ in the presence of free TBBT thiol. This study explored the use of real-time monitoring of the exchange kinetics process by advanced mass spectrometric and optical spectroscopic analyses. This method was also effectively used for the synthesis of alloy NCs such as $Au_{24-x}Ag_x(TBBM)_{20}$ ($x \approx 1$) (where TBBM = *tert*-butylbenzyl mercaptan) (*148*), $Au_{36-x}Ag_x(TBBT)_{24}$ ($x$ = 1–8) (*149*), and $Au_{38-x}Cu_x(2,4\text{-}(CH_3)_2C_6H_3S)_{24}$ ($x$ = 0–6) (*150*), as well as $Au_{20}Ag_1(TBM)_{15}$, $Au_{21-x}Ag_x(TBM)_{15}$ ($x$ = 4–8), $Au_{21-x}Cu_x(TBM)_{15}$ ($x$ = 0, 1), and $Au_{21-x}Cu_x(TBM)_{15}$ ($x$ = 2–5) (where TBM = *tert*-butyl mercaptan) (*151*). Ligand exchange of small-size, phosphine-protected Au NCs with PhSeH ligands was successfully achieved by Song et al. (*152*) Rodlike $Au_{25}(PPh_3)_{10}(SePh)_5Cl_2$ NCs with 1+ or 2+ valence states were obtained. These Se–$Au_{25}$ clusters were synthesized by reacting $Au_m(PPh_3)_n$ clusters with PhSeH ligands under different conditions. Specifically, ligand exchange of $Au_m(PPh_3)_n$ at 28 °C in ethanol yielded Se–$Au_{25}$ with a 1+ valence state, whereas ligand exchange at 0 °C in $CH_2Cl_2$ resulted in Se–$Au_{25}$ with a 2+ valence state. The oxidation of $[Au_{25}(PPh_3)_{10}(SePh)_5Cl_2]^+$ with $H_2O_2$ gave rise to the 2+ charged NC. The synthesis process and the determined structures of NCs are illustrated in panels a and b, respectively, of Figure 16. A two-phase ligand-exchange method for the preparation of water-soluble AuAg NCs protected by tiopronin from $Au_xAg_{44-x}$ alloy precursors was reported recently (*153*). In this case, the synthesis of AuAg alloy precursors coprotected by alkyne and phosphine ligands was performed initially, followed by a two-phase ligand-exchange process (see Figure 16c).

This method can be applied to various water-soluble ligands, such as tiopronin, captopril, *N*-acetyl-l-cysteine, 4-mercaptobenzoic acid, glutathione, and mercaptosuccinic acid. According to the studies, the driving forces for the structural transformation induced by ligand exchange was found to be the alternation in coordination modes between metals and ligands (*154*). There are some drawbacks that need to be addressed to improve the effectiveness of this method, including controlling the reaction conditions to produce more new NCs and dictating the precise ligand-exchange process through a stepwise ligand-by-ligand substitution mode.

### *2.2.2. Atom-Trapping Method*

The atom-trapping method is a characteristic top-down method that requires a supply of mobile atoms and a suitable support capable of binding the mobile species. Generally, atomic and nanoscale

catalyst preparation is successful for limited metal-containing catalysts. Often, the metals adsorbed on oxides undergo aggregation during the synthesis, particularly at high temperatures, resulting in low catalytic activities because of the loss of surface area (*155*, *156*). To overcome this issue, Carrillo et al. proposed an atom-trapping strategy using PdO, which effectively trapped mobile $PtO_2$ and formed a Pt–Pd alloy by physical vapor deposition in air (*157*). Similarly, Jones et al. (*158*) made use of mobile $CeO_2$ to trap Pt atoms on its surface to form a sinter-resistant, atomically dispersed single-atom platinum-on-ceria material. This strategy involves the supply of mobile atoms and a support that can bind the mobile species. The defects on oxides trapped in $PtO_2$ can migrate by means of the gas phase, which plays a vital role in stabilizing the catalyst. Later, using this method, sinter-resistant SACs based on Pd, Au, Ni, and Cu were reported by various research groups (*46*, *48*, *55*). In contrast, the ceria support is unique in its ability to trap Pt species. Xiong et al. studied Pt–Sn/$CeO_2$ catalysts for propane dehydrogenation, where ceria supports showed a unique ability to trap ionic platinum, providing exceptional stability for isolated single atoms of Pt (*159*). Under reducing conditions, Pt atoms were found to be mobile and alloyed with the Sn, forming bimetallic NPs in the working catalyst, as shown in Figure 17.

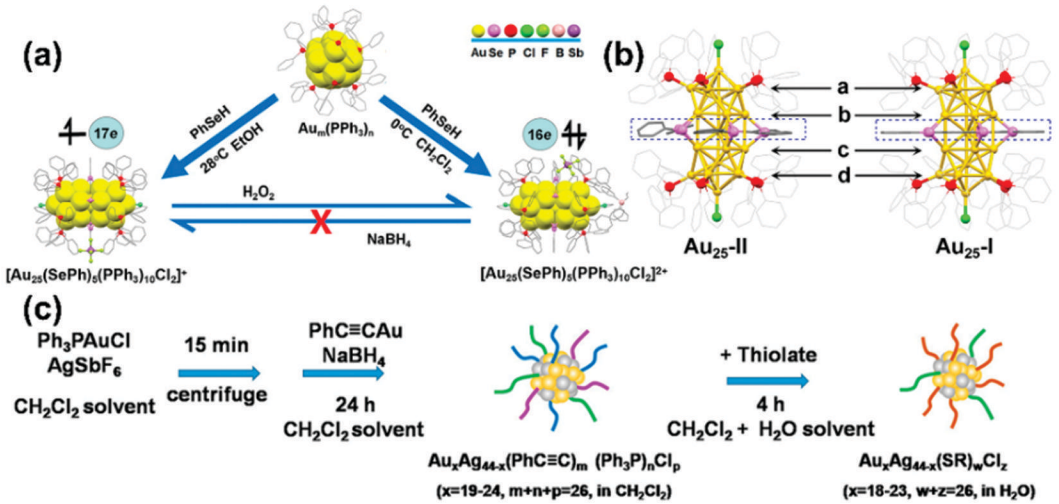


*Figure 16. (a) Synthesis of rodlike $Au_{25}(PPh_3)_{10}(SePh)_5Cl_2$ NCs with 1+ and 2+ valence states. (b) Crystal structures of the $Au_{25}$-I and $Au_{25}$-II NCs (color labels: Au, yellow; P, red; Cl, green; and Se, violet; C atoms are in wireframe for clarity). Panels a and b reproduced with permission from reference* (*152*). *Copyright 2016 American Chemical Society. (c) Two-phase ligand-exchange method for the preparation of water-soluble AuAg NCs. Reproduced with permission from reference* (*153*). *Copyright 2018 American Chemical Society.*

Here, the Pt formed single-atom species, whereas the Sn remained in the form of $SnO_2$ particles. Conversely, the regeneration of the catalyst was observed under mild oxidative conditions. This demonstrated the ease of ceria-supported catalysts in re-creating the single-atom species by regeneration under mild oxidation conditions.

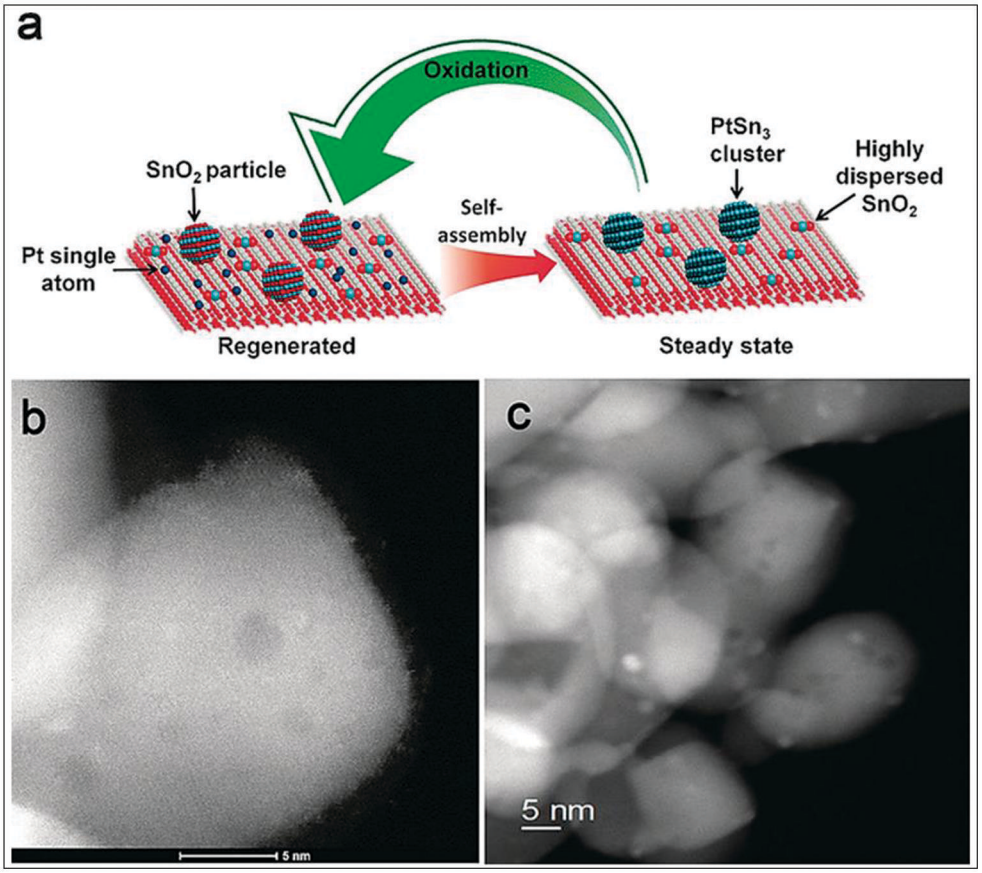


*Figure 17. (a) Schematic of the self-assembly and regeneration processes of Pt–Sn NCs in propane dehydrogenation at 680 °C. (b) STEM image of regenerated Pt–Sn/$CeO_2$ catalyst (air, 580 °C). (c) STEM image of spent Pt–Sn/$CeO_2$ catalyst after propane dehydrogenation at 680 °C. Reproduced with permission from reference* (*159*)*. Copyright 2017 Wiley-VCH.*

## 3. Conclusions

This chapter has summarized the latest research progress on the synthesis of atomic and nanoscale catalysts. Various synthesis protocols have been developed in recent years. However, economically scalable synthesis methods are essential for high-quality, large-scale preparation and the application of monodisperse metal catalysts. The stability of nanostructured catalysts is a serious issue that needs to be addressed. The development of well-defined subnanometer and single-atom materials resulted in the formation of highly effective and selective heterogeneous catalysts. However, many of these catalytic entities cannot retain atomic-level dispersion under harsh reaction conditions, thus impeding the application of laboratory-bench discoveries to realistic large industrial-scale processes. The identification of the true structure of the active site is essential for the fundamental understanding and design of optimized and improved SACs. Supports also play a crucial role in defining the catalytic performance of atomically dispersed SACs, as the binding of ISAs with the support should be very strong to overcome aggregation. The construction of ISAs demands a careful balance between metal–metal and metal–support bonding strengths, as it involves high-energy bond breaking and re-forming. These activation energies may lead to the diffusion of single metal atoms, which can coalesce to cause aggregation. Thus, atomic-scale information on single-

atom diffusion on supports during reactions is essential in understanding sintering mechanisms and designing high-performance catalytic systems. The aggregation can be avoided by lowering the metal loading on the solid supports by the spatial distribution of metal precursors. However, ISA catalysts with the low metal loadings are unsuitable for practical catalytic applications. Defect engineering can potentially be explored so that single metal atoms can be preferentially exposed at surface sites. This leads to additional doping sites for the metal as well as for heteroatoms and substantially enhances the SAC's catalytic efficiency. Alternatively, novel synthetic strategies that can minimize metal precursor exposure to high-energy environmental conditions should be developed for economically scalable synthesis at the large industrial scale. Overall, the enhancement, tuning, and mechanistic understanding of metal–support interactions and the identification of preferential support sites for metal anchoring are needed to achieve improved highly loaded, stable supported single-metal-atom catalysts with enhanced activity and selectivity.

## Acknowledgments

R.K.S. dedicates this book chapter to his supervisor, Prof. Ashoka G. Samuelson, Department of Inorganic and Physical Chemistry, Indian Institute of Science Bangalore, on the occasion of his 64th birthday. The authors thank DBT-PAN IIT Centre for Bioenergy (BT/EB/PANIIT/2012) for financial support.

## References

1. Fernández, E.; Boronat, M. Sub Nanometer Clusters in Catalysis. *J. Phys.: Condens. Matter* **2019**, *31*, 013002.
2. Lu, Y.; Chen, W. Sub-Nanometre Sized Metal Clusters: From Synthetic Challenges to the Unique Property Discoveries. *Chem. Soc. Rev.* **2012**, *41*, 3594–3623.
3. Yang, L.-L.; Wang, H.-J.; Wang, J.; Li, Y.; Zhang, W.; Lu, T.-B. A Graphdiyne-Based Carbon Material for Electroless Deposition and Stabilization of Sub-Nanometric Pd Catalysts with Extremely High Catalytic Activity. *J. Mater. Chem. A* **2019**, *7*, 13142–13148.
4. Fernández, E.; Liu, L.; Boronat, M.; Arenal, R.; Concepcion, P.; Corma, A. Low-Temperature Catalytic NO Reduction with CO by Subnanometric Pt Clusters. *ACS Catal.* **2019**, *9*, 11530–11541.
5. Yang, X.-F.; Wang, A.; Qiao, B.; Li, J.; Liu, J.; Zhang, T. Single-Atom Catalysts: A New Frontier in Heterogeneous Catalysis. *Acc. Chem. Res.* **2013**, *46*, 1740–1748.
6. Cheng, N.; Zhang, L.; Doyle-Davis, K.; Sun, X. Single-Atom Catalysts: From Design to Application. *Electrochem. Energy Rev.* **2019**, *2*, 539–573.
7. Du, Y.; Sheng, H.; Astruc, D.; Zhu, M. Atomically Precise Noble Metal Nanoclusters as Efficient Catalysts: A Bridge between Structure and Properties. *Chem. Rev.* **2020**, *120*, 526–622.
8. Li, Z.; Ji, S.; Liu, Y.; Cao, X.; Tian, S.; Chen, Y.; Niu, Z.; Li, Y. Well-Defined Materials for Heterogeneous Catalysis: From Nanoparticles to Isolated Single-Atom Sites. *Chem. Rev.* **2020**, *120*, 623–682.
9. Ji, S.; Chen, Y.; Wang, X.; Zhang, Z.; Wang, D.; Li, Y. Chemical Synthesis of Single Atomic Site Catalysts. *Chem. Rev.* [Online early access]. DOI: 10.1021/acs.chemrev.9b00818. Published online Apr 3, 2020. https://doi.org/10.1021/acs.chemrev.9b00818.

10. Brust, M.; Walker, M.; Bethell, D.; Schiffrin, D. J.; Whyman, R. Synthesis of Thiol-Derivatised Gold Nanoparticles in a Two-Phase Liquid–Liquid System. *J. Chem. Soc., Chem. Commun.* **1994**, 801–802.
11. Li, Y.; Zaluzhna, O.; Xu, B.; Gao, Y.; Modest, J. M.; Tong, Y. J. Mechanistic Insights into the Brust–Schiffrin Two-Phase Synthesis of Organo-Chalcogenate-Protected Metal Nanoparticles. *J. Am. Chem. Soc.* **2012**, *133*, 6498–6498.
12. Perala, S. R. K.; Kumar, S. On the Mechanism of Metal Nanoparticle Synthesis in the Brust–Schiffrin Method. *Langmuir* **2013**, *29*, 9863–9873.
13. Brust, M.; Fink, J.; Bethell, D.; Schiffrin, D. J.; Kiely, C. Synthesis and Reactions of Functionalised Gold Nanoparticles. *J. Chem. Soc., Chem. Commun.* **1995**, 1655–1656.
14. Qian, H.; Jin, R. Ambient Synthesis of $Au_{144}(SR)_{60}$ Nanoclusters in Methanol. *Chem. Mater.* **2011**, *23*, 2209–2217.
15. Tsunoyama, H.; Negishi, Y.; Tsukuda, T. Chromatographic Isolation of "Missing" $Au_{55}$ Clusters Protected by Alkanethiolates. *J. Am. Chem. Soc.* **2006**, *128*, 6036–6037.
16. Branham, M. R.; Douglas, A. D.; Mills, A. J.; Tracy, J. B.; White, P. S.; Murray, R. W. Arylthiolate-Protected Silver Quantum Dots. *Langmuir* **2006**, *22*, 11376–11383.
17. Devadas, M. S.; Kwak, K.; Park, J.-W.; Choi, J.-H.; Jun, C.-H.; Sinn, E.; Ramakrishna, G.; Lee, D. Directional Electron Transfer in Chromophore-Labeled Quantum-Sized $Au_{25}$ Clusters: $Au_{25}$ as an Electron Donor. *J. Phys. Chem. Lett.* **2010**, *1*, 1497–1503.
18. Song, Y.; Harper, A. S.; Murray, R. W. Ligand Heterogeneity on Monolayer-Protected Gold Clusters. *Langmuir* **2005**, *21*, 5492–5500.
19. Venzo, A.; Antonello, S.; Gascón, J. A.; Guryanov, I.; Leapman, R. D.; Perera, N. V.; Sousa, A.; Zamuner, M.; Zanella, A.; Maran, F. Effect of the Charge State ($z = -1$, 0, $+1$) on the Nuclear Magnetic Resonance of Monodisperse $Au_{25}[S(CH_2)_2Ph]_{18}^{z}$ Clusters. *Anal. Chem.* **2011**, *83*, 6355–6362.
20. Castro, E. G.; Salvatierra, R. V.; Schreiner, W. H.; Oliveira, M. M.; Zarbin, A. J. G. Dodecanethiol-Stabilized Platinum Nanoparticles Obtained by a Two-Phase Method: Synthesis, Characterization, Mechanism of Formation, and Electrocatalytic Properties. *Chem. Mater.* **2010**, *22*, 360–370.
21. Wu, Z.; Lanni, E.; Chen, W.; Bier, M. E.; Ly, D.; Jin, R. High Yield, Large Scale Synthesis of Thiolate-Protected $Ag_7$ Clusters. *J. Am. Chem. Soc.* **2009**, *131*, 16672–16674.
22. Ang, T. P.; Wee, T. S. A.; Chin, W. S. Three-Dimensional Self-Assembled Monolayer (3D SAM) of *n*-Alkanethiols on Copper Nanoclusters. *J. Phys. Chem. B* **2004**, *108*, 11001–11010.
23. Zhu, M.; Lanni, E.; Garg, N.; Bier, M. E.; Jin, R. Kinetically Controlled, High-Yield Synthesis of $Au_{25}$ Clusters. *J. Am. Chem. Soc.* **2008**, *130*, 1138–1139.
24. Wu, Z.; Suhan, J.; Jin, R. One-Pot Synthesis of Atomically Monodisperse, Thiol-Functionalized $Au_{25}$ Nanoclusters. *J. Mater. Chem.* **2009**, *19*, 622–626.
25. Goulet, P. J. G.; Lennox, R. B. New Insights into Brust−Schiffrin Metal Nanoparticle Synthesis. *J. Am. Chem. Soc.* **2010**, *132*, 9582–9584.
26. Li, Y.; Zaluzhna, O.; Xu, B.; Gao, Y.; Modest, J. M.; Tong, Y. J. Mechanistic Insights into the Brust−Schiffrin Two-Phase Synthesis of Organo-Chalcogenate-Protected Metal Nanoparticles. *J. Am. Chem. Soc.* **2011**, *133*, 2092–2095.

27. Bartlett, P. A.; Bauer, B.; Singer, S. J. Synthesis of Water-Soluble Undecagold Cluster Compounds of Potential Importance in Electron Microscopic and Other Studies of Biological Systems. *J. Am. Chem. Soc.* **1978**, *100*, 5085–5089.
28. Schmid, G.; Pfeil, R.; Boese, R.; Bandermann, F.; Meyer, S.; Calis, G. H. M.; van der Velden, J. W. A. $Au_{55}[P(C_6H_5)_3]_{12}CI_6$ — ein Goldcluster ungewöhnlicher Größe. *Chem. Ber.* **1981**, *114*, 3634.
29. Weare, W. W.; Reed, S. M.; Warner, M. G.; Hutchison, J. E. Improved Synthesis of Small ($d_{CORE} \approx 1.5$ nm) Phosphine-Stabilized Gold Nanoparticles. *J. Am. Chem. Soc.* **2000**, *122*, 12890–12891.
30. Zhang, H.-F.; Stender, M.; Zhang, R.; Wang, C.; Li, J.; Wang, L.-S. Toward the Solution Synthesis of the Tetrahedral $Au_{20}$ Cluster. *J. Phys. Chem. B* **2004**, *108*, 12259–12263.
31. Bertino, M. F.; Sun, Z.-M.; Zhang, R.; Wang, L.-S. Facile Syntheses of Monodisperse Ultrasmall Au Clusters. *J. Phys. Chem. B* **2006**, *110*, 21416–21418.
32. Pettibone, J. M.; Hudgens, J. W. Synthetic Approach for Tunable, Size-Selective Formation of Monodisperse, Diphosphine-Protected Gold Nanoclusters. *J. Phys. Chem. Lett.* **2010**, *1*, 2536–2540.
33. Huang, T.; Huang, L.; He, W.; Song, X.; Sun, Z.; Jiang, Y.; Pan, G.; Wei, S. Ammonia-Induced Size Convergence of Atomically Monodisperse $Au_6$ Nanoclusters. *J. Phys. Chem. C* **2018**, *122*, 6405–6411.
34. Shem, P. M.; Sardar, R.; Shumaker-Parry, J. S. One-Step Synthesis of Phosphine-Stabilized Gold Nanoparticles Using the Mild Reducing Agent 9-BBN. *Langmuir* **2009**, *25*, 13279–13283.
35. Jin, S.; Du, W.; Wang, S.; Kang, X.; Chen, M.; Hu, D.; Chen, S.; Zou, X.; Sun, G.; Zhu, M. Thiol-Induced Synthesis of Phosphine-Protected Gold Nanoclusters with Atomic Precision and Controlling the Structure by Ligand/Metal Engineering. *Inorg. Chem.* **2017**, *56*, 11151–11159.
36. Wang, Q.; Astruc, D. State of the Art and Prospects in Metal–Organic Framework (MOF)-Based and MOF-Derived Nanocatalysis. *Chem. Rev.* **2020**, *120*, 1438–1511.
37. Sudarsanam, P.; Zhong, R.; Van den Bosch, S.; Coman, S. M.; Parvulescu, V. I.; Sels, B. F. Functionalised Heterogeneous Catalysts for Sustainable Biomass Valorisation. *Chem. Soc. Rev.* **2018**, *47*, 8349–8402.
38. Zhou, H.-C.; Long, J. R.; Yaghi, O. M. Introduction to Metal–Organic Frameworks. *Chem. Rev.* **2012**, *112*, 673–674.
39. Yin, P.; Yao, T.; Wu, Y.; Zheng, L.; Lin, Y.; Liu, W.; Ju, H.; Zhu, J.; Hong, X.; Deng, Z.; Zhou, G.; Wei, S.; Li, Y. Single Cobalt Atoms with Precise N-Coordination as Superior Oxygen Reduction Reaction Catalysts. *Angew. Chem., Int. Ed.* **2016**, *55*, 10800–10805.
40. Wang, X.; Chen, Z.; Zhao, X.; Yao, T.; Chen, W.; You, R.; Zhao, C.; Wu, G.; Wang, J.; Huang, W.; Yang, J.; Hong, X.; Wei, S.; Wu, Y.; Li, Y. Regulation of Coordination Number over Single Co Sites: Triggering the Efficient Electroreduction of $CO_2$. *Angew. Chem., Int. Ed.* **2018**, *57*, 1944–1948.
41. Wang, J.; Huang, Z.; Liu, W.; Chang, C.; Tang, H.; Li, Z.; Chen, W.; Jia, C.; Yao, T.; Wei, S.; Wu, Y.; Li, Y. Design of N-Coordinated Dual-Metal Sites: A Stable and Active Pt-Free Catalyst for Acidic Oxygen Reduction Reaction. *J. Am. Chem. Soc.* **2017**, *139*, 17281–17284.

42. Chen, Y.; Ji, S.; Wang, Y.; Dong, J.; Chen, W.; Li, Z.; Shen, R.; Zheng, L.; Zhuang, Z.; Wang, D.; Li, Y. Isolated Single Iron Atoms Anchored on N-Doped Porous Carbon as an Efficient Electrocatalyst for the Oxygen Reduction Reaction. *Angew. Chem., Int. Ed.* **2017**, *56*, 6937–6941.
43. Xiao, M.; Zhu, J.; Ma, L.; Jin, Z.; Ge, J.; Deng, X.; Hou, Y.; He, Q.; Li, J.; Jia, Q.; Mukerjee, S.; Yang, R.; Jiang, Z.; Su, D.; Liu, C.; Xing, W. Microporous Framework Induced Synthesis of Single-Atom Dispersed Fe-N-C Acidic ORR Catalyst and Its in Situ Reduced Fe-$N_4$ Active Site Identification Revealed by X-ray Absorption Spectroscopy. *ACS Catal.* **2018**, *8*, 2824–2832.
44. Wang, X. X.; Cullen, D. A.; Pan, Y.-T.; Hwang, S.; Wang, M.; Feng, Z.; Wang, J.; Engelhard, M. H.; Zhang, H.; He, Y.; Shao, Y.; Su, D.; More, K. L.; Spendelow, J. S.; Wu, G. Nitrogen-Coordinated Single Cobalt Atom Catalysts for Oxygen Reduction in Proton Exchange Membrane Fuel Cells. *Adv. Mater.* **2018**, *30*, 1706758.
45. Zhao, C.; Dai, X.; Yao, T.; Chen, W.; Wang, X.; Wang, J.; Yang, J.; Wei, S.; Wu, Y.; Li, Y. Ionic Exchange of Metal–Organic Frameworks to Access Single Nickel Sites for Efficient Electroreduction of $CO_2$. *J. Am. Chem. Soc.* **2017**, *139*, 8078–8081.
46. Yang, J.; Qiu, Z.; Zhao, C.; Wei, W.; Chen, W.; Li, Z.; Qu, Y.; Dong, J.; Luo, J.; Li, Z.; Wu, Y. In Situ Thermal Atomization to Convert Supported Nickel Nanoparticles into Surface-Bound Nickel Single-Atom Catalysts. *Angew. Chem., Int. Ed.* **2018**, *130*, 14095–14100.
47. Ji, S.; Chen, Y.; Fu, Q.; Chen, Y.; Dong, J.; Chen, W.; Li, Z.; Wang, Y.; Gu, L.; He, W.; Chen, C.; Peng, Q.; Huang, Y.; Duan, X.; Wang, D.; Draxl, C.; Li, Y. Confined Pyrolysis within Metal–Organic Frameworks to Form Uniform $Ru_3$ Clusters for Efficient Oxidation of Alcohols. *J. Am. Chem. Soc.* **2017**, *139*, 9795–9798.
48. Wei, S.; Li, A.; Liu, J.-C.; Li, Z.; Chen, W.; Gong, Y.; Zhang, Q.; Cheong, W.-C.; Wang, Y.; Zheng, L.; Xiao, H.; Chen, C.; Wang, D.; Peng, Q.; Gu, L.; Han, X.; Li, J.; Li, Y. Direct Observation of Noble Metal Nanoparticles Transforming to Thermally Stable Single Atoms. *Nat. Nanotechnol.* **2018**, *13*, 856–861.
49. Zhang, Z.; Sun, J.; Wang, F.; Dai, L. Efficient Oxygen Reduction Reaction (ORR) Catalysts Based on Single Iron Atoms Dispersed on a Hierarchically Structured Porous Carbon Framework. *Angew. Chem., Int. Ed.* **2018**, *57*, 9038–9043.
50. Jiao, L.; Wan, G.; Zhang, R.; Zhou, H.; Yu, S.-H.; Jiang, H.-L. From Metal–Organic Frameworks to Single-Atom Fe Implanted N-Doped Porous Carbons: Efficient Oxygen Reduction in Both Alkaline and Acidic Media. *Angew. Chem., Int. Ed.* **2018**, *57*, 8525–8529.
51. Zhang, M.; Wang, Y.-G.; Chen, W.; Dong, J.; Zheng, L.; Luo, J.; Wan, J.; Tian, S.; Cheong, W.-C.; Wang, D.; Li, Y. Metal (Hydr)oxides@Polymer Core–Shell Strategy to Metal Single-Atom Materials. *J. Am. Chem. Soc.* **2017**, *139*, 10976–10979.
52. Chen, Y.; Ji, S.; Zhao, S.; Chen, W.; Dong, J.; Cheong, W.-C.; Shen, R.; Wen, X.; Zheng, L.; Rykov, A. I.; Cai, S.; Tang, H.; Zhuang, Z.; Chen, C.; Peng, Q.; Wang, D.; Li, Y. Enhanced Oxygen Reduction with Single-Atomic-Site Iron Catalysts for a Zinc-Air Battery and Hydrogen-Air Fuel Cell. *Nat. Commun.* **2018**, *9*, 5422.
53. Chen, W.; Pei, J.; He, C.-T.; Wan, J.; Ren, H.; Wang, Y.; Dong, J.; Wu, K.; Cheong, W.-C.; Mao, J.; Zheng, X.; Yan, W.; Zhuang, Z.; Chen, C.; Peng, Q.; Wang, D.; Li, Y. Single Tungsten Atoms Supported on MOF-Derived N-Doped Carbon for Robust Electrochemical Hydrogen Evolution. *Adv. Mater.* **2018**, *30*, 1800396.

54. Wang, X.; Chen, W.; Zhang, L.; Yao, T.; Liu, W.; Lin, Y.; Ju, H.; Dong, J.; Zheng, L.; Yan, W.; Zheng, X.; Li, Z.; Wang, X.; Yang, J.; He, D.; Wang, Y.; Deng, Z.; Wu, Y.; Li, Y. Uncoordinated Amine Groups of Metal–Organic Frameworks to Anchor Single Ru Sites as Chemoselective Catalysts toward the Hydrogenation of Quinoline. *J. Am. Chem. Soc.* **2017**, *139*, 9419–9422.
55. Qu, Y.; Li, Z.; Chen, W.; Lin, Y.; Yuan, T.; Yang, Z.; Zhao, C.; Wang, J.; Zhao, C.; Wang, X.; Zhou, F.; Zhuang, Z.; Wu, Y.; Li, Y. Direct Transformation of Bulk Copper into Copper Single Sites via Emitting and Trapping of Atoms. *Nat. Catal.* **2018**, *1*, 781–786.
56. Deng, Y.; Chi, B.; Li, J.; Wang, G.; Zheng, L.; Shi, X.; Cui, Z.; Du, L.; Liao, S.; Zang, K.; Luo, J.; Hu, Y.; Sun, X. Atomic Fe-Doped MOF-Derived Carbon Polyhedrons with High Active-Center Density and Ultra-High Performance toward PEM Fuel Cells. *Adv. Energy Mater.* **2019**, *9*, 1802856.
57. Zhu, Y.-J.; Chen, F. Microwave-Assisted Preparation of Inorganic Nanostructures in Liquid Phase. *Chem. Rev.* **2014**, *114*, 6462–6555.
58. Bilecka, I.; Niederberger, M. Microwave Chemistry for Inorganic Nanomaterials Synthesis. *Nanoscale* **2010**, *2*, 1358–1374.
59. Krishnapriya, R.; Praneetha, S.; Vadivel Murugan, A. Microwave-Solvothermal Synthesis of Various $TiO_2$ Nano-Morphologies with Enhanced Efficiency by Incorporating Ni Nanoparticles in an Electrolyte for Dye-Sensitized Solar Cells. *Inorg. Chem. Front.* **2017**, *4*, 1665–1678.
60. Gerbec, J. A.; Magana, D.; Washington, A.; Strouse, G. F. Microwave-Enhanced Reaction Rates for Nanoparticle Synthesis. *J. Am. Chem. Soc.* **2005**, *127*, 15791–15800.
61. Tu, W.; Liu, H. Continuous Synthesis of Colloidal Metal Nanoclusters by Microwave Irradiation. *Chem. Mater.* **2000**, *12*, 564–567.
62. Roberts, B. A.; Strauss, C. R. Toward Rapid, "Green", Predictable Microwave-Assisted Synthesis. *Acc. Chem. Res.* **2005**, *38*, 653–661.
63. Liu, S.; Lu, F.; Zhu, J.-J. Highly Fluorescent Ag Nanoclusters: Microwave-Assisted Green Synthesis and $Cr^{3+}$ Sensing. *Chem. Commun.* **2011**, *47*, 2661–2663.
64. Kawasaki, H.; Kosaka, Y.; Myoujin, Y.; Narushima, T.; Yonezawa, T.; Arakawa, R. Microwave-Assisted Polyol Synthesis of Copper Nanocrystals without Using Additional Protective Agents. *Chem. Commun.* **2011**, *47*, 7740–7742.
65. Fei, H.; Dong, J.; Wan, C.; Zhao, Z.; Xu, X.; Lin, Z.; Wang, Y.; Liu, H.; Zang, K.; Luo, J.; Zhao, S.; Hu, W.; Yan, W.; Shakir, I.; Huang, Y.; Duan, X. Microwave-Assisted Rapid Synthesis of Graphene-Supported Single Atomic Metals. *Adv. Mater.* **2018**, *30*, 1802146.
66. Fei, H.; Dong, J.; Chen, D.; Hu, T.; Duan, X.; Shakir, I.; Huang, Y.; Duan, X. Single Atom Electrocatalysts Supported on Graphene or Graphene-Like Carbons. *Chem. Soc. Rev.* **2019**, *48*, 5207–5241.
67. Peyser, L. A.; Vinson, A. E.; Bartko, A. P.; Dickson, R. M. Photoactivated Fluorescence from Individual Silver Nanoclusters. *Science* **2001**, *291*, 103–106.
68. Liu, P.; Zhao, Y.; Qin, R.; Mo, S.; Chen, G.; Gu, L.; Chevrier, D. M.; Zhang, P.; Guo, Q.; Zang, D.; Wu, B.; Fu, G.; Zheng, N. Photochemical Route for Synthesizing Atomically Dispersed Palladium Catalysts. *Science* **2016**, *352*, 797–800.
69. Wang, Q.; Zhang, D.; Chen, Y.; Fu, W.-F.; Lv, X.-J. Single-Atom Catalysts for Photocatalytic Reactions. *ACS Sustainable Chem. Eng.* **2019**, *7*, 6430–6443.

70. Sui, Y.; Liu, S.; Li, T.; Liu, Q.; Jiang, T.; Guo, Y.; Luo, J.-L. Atomically dispersed Pt on specific $TiO_2$ facets for photocatalytic $H_2$ evolution. *J. Catal.* **2017**, *353*, 250–255.
71. Wei, H.; Wu, H.; Huang, K.; Ge, B.; Ma, J.; Lang, J.; Zu, D.; Lei, M.; Yao, Y.; Guo, W.; Wu, H. Ultralow-Temperature Photochemical Synthesis of Atomically Dispersed Pt Catalysts for the Hydrogen Evolution Reaction. *Chem. Sci.* **2019**, *10*, 2830–2836.
72. Li, T.; Liu, J.; Song, Y.; Wang, F. Photochemical Solid-Phase Synthesis of Platinum Single Atoms on Nitrogen-Doped Carbon with High Loading as Bifunctional Catalysts for Hydrogen Evolution and Oxygen Reduction Reactions. *ACS Catal.* **2018**, *8*, 8450–8458.
73. Wei, H.; Huang, K.; Wang, D.; Zhang, R.; Ge, B.; Ma, J.; Wen, B.; Zhang, S.; Li, Q.; Lei, M.; Zhang, C.; Irawan, J.; Liu, L.-M.; Wu, H. Iced Photochemical Reduction to Synthesize Atomically Dispersed Metals by Suppressing Nanocrystal Growth. *Nat. Commun.* **2017**, *8*, 1490.
74. Christensen, S. T.; Elam, J. W.; Rabuffetti, F. A.; Ma, Q.; Weigand, S. J.; Lee, B.; Seifert, S.; Stair, P. C.; Poeppelmeier, K. R.; Hersam, M. C.; Bedzyk, M. J. Controlled Growth of Platinum Nanoparticles on Strontium Titanate Nanocubes by Atomic Layer Deposition. *Small* **2009**, *5*, 750–757.
75. Lu, J.; Elam, J. W.; Stair, P. C. Synthesis and Stabilization of Supported Metal Catalysts by Atomic Layer Deposition. *Acc. Chem. Res.* **2013**, *46*, 1806–1815.
76. Suntola, T.; Hyvarinen, J. Atomic Layer Epitaxy. *Annu. Rev. Mater. Sci.* **1985**, *15*, 177–195.
77. Lu, J.; Stair, P. C. Low-Temperature ABC-Type Atomic Layer Deposition: Synthesis of Highly Uniform Ultrafine Supported Metal Nanoparticles. *Angew. Chem., Int. Ed.* **2010**, *49*, 2547–2551.
78. Stambula, S.; Gauquelin, N.; Bugnet, M.; Gorantla, S.; Turner, S.; Sun, S.; Liu, J.; Zhang, G.; Sun, X.; Botton, G. A. Chemical Structure of Nitrogen-Doped Graphene with Single Platinum Atoms and Atomic Clusters as a Platform for the PEMFC Electrode. *J. Phys. Chem. C* **2014**, *118*, 3890–3900.
79. Sun, S.; Zhang, G.; Gauquelin, N.; Chen, N.; Zhou, J.; Yang, S.; Chen, W.; Meng, X.; Geng, D.; Banis, M. N.; Li, R.; Ye, S.; Knights, S.; Botton, G. A.; Sham, T.-K.; Sun, X. Single-Atom Catalysis Using Pt/Graphene Achieved through Atomic Layer Deposition. *Sci. Rep.* **2013**, *3*, 1775.
80. Yan, H.; Cheng, H.; Yi, H.; Lin, Y.; Yao, T.; Wang, C.; Li, J.; Wei, S.; Lu, J. Single-Atom $Pd_1$/Graphene Catalyst Achieved by Atomic Layer Deposition: Remarkable Performance in Selective Hydrogenation of 1,3-Butadiene. *J. Am. Chem. Soc.* **2015**, *137*, 10484–10487.
81. Liu, J. Catalysis by Supported Single Metal Atoms. *ACS Catal.* **2017**, *7*, 34–59.
82. López-Quintela, M. A. Synthesis of Nanomaterials in Microemulsions: Formation Mechanisms and Growth Control. *Curr. Opin. Colloid Interface Sci.* **2003**, *8*, 137–144.
83. López-Quintela, M. A.; Tojo, C.; Blanco, M. C.; Garcıa Rio, L.; Leis, J. R. Microemulsion Dynamics and Reactions in Microemulsions. *Curr. Opin. Colloid Interface Sci.* **2004**, *9*, 264–278.
84. Capek, I. Preparation of Metal Nanoparticles in Water-in-Oil (W/O) Microemulsions. *Adv. Colloid Interface Sci.* **2004**, *110*, 49–74.
85. Qiu, S.; Dong, J.; Chen, G. Preparation of Cu Nanoparticles from Water-in-Oil Microemulsions. *J. Colloid Interface Sci.* **1999**, *216*, 230–234.

86. Ledo-Suárez, A.; Rivas, J.; Rodríguez-Abreu, C. F.; Rodríguez, M. J.; Pastor, E.; Hernández-Creus, A.; Oseroff, S. B.; López-Quintela, M. A. Facile Synthesis of Stable Subnanosized Silver Clusters in Microemulsions. *Angew. Chem., Int. Ed.* **2007**, *46*, 8823–8827.
87. Vázquez-Vázquez, C.; Bañobre-López, M.; Mitra, A.; López-Quintela, M. A.; Rivas, J. Synthesis of Small Atomic Copper Clusters in Microemulsions. *Langmuir* **2009**, *25*, 8208–8216.
88. Chen, D.-H.; Wu, S.-H. Synthesis of Nickel Nanoparticles in Water-in-Oil Microemulsions. *Chem. Mater.* **2000**, *12*, 1354–1360.
89. Kawasaki, H.; Yamamoto, H.; Fujimori, H.; Arakawa, R.; Iwasaki, Y.; Inada, M. Stability of the DMF-Protected Au Nanoclusters: Photochemical, Dispersion, and Thermal Properties. *Langmuir* **2010**, *26*, 5926–5933.
90. Kawasaki, H.; Yamamoto, H.; Fujimori, H.; Arakawa, R.; Inada, M.; Iwasaki, Y. Surfactant-Free Solution Synthesis of Platinum Subnanoclusters. *Chem. Commun.* **2010**, *46*, 3759–3761.
91. Hyotanishi, M.; Isomura, Y.; Yamamoto, H.; Kawasaki, H.; Obora, Y. Surfactant-Free Synthesis of Palladium Nanoclusters for Their Use in Catalytic Cross-Coupling Reactions. *Chem. Commun.* **2011**, *47*, 5750–5752.
92. Cui, Z.; Coletta, C.; Dazzi, A.; Lefrançois, P.; Gervais, M.; Néron, S.; Remita, S. Radiolytic Method as a Novel Approach for the Synthesis of Nanostructured Conducting Polypyrrole. *Langmuir* **2014**, *30*, 14086–14094.
93. Grand, J.; Ferreira, S. R.; de Waele, V.; Mintova, S.; Nenoff, T. M. Nanoparticle Alloy Formation by Radiolysis. *J. Phys. Chem. C* **2018**, *122*, 12573–12588.
94. Linnert, T.; Mulvaney, P.; Henglein, A.; Weller, H. Long-Lived Nonmetallic Silver Clusters in Aqueous Solution: Preparation and Photolysis. *J. Am. Chem. Soc.* **1990**, *112*, 4657–4664.
95. Ershov, B. G.; Henglein, A. Reduction of $Ag^+$ on Polyacrylate Chains in Aqueous Solution. *J. Phys. Chem. B* **1998**, *102*, 10663–10666.
96. Mulvaney, P.; Henglein, A. Formation of Unstabilized Oligomeric Silver Clusters During the Reduction of $Ag^+$ Ions in Aqueous Solution. *Chem. Phys. Lett.* **1990**, *168*, 391–394.
97. Reetz, M. T.; Helbig, W. Size-Selective Synthesis of Nanostructured Transition Metal Clusters. *J. Am. Chem. Soc.* **1994**, *116*, 7401–7402.
98. Vilar-Vidal, N.; Blanco, M. C.; López-Quintela, M. A.; Rivas, J.; Serra, C. Electrochemical Synthesis of Very Stable Photoluminescent Copper Clusters. *J. Phys. Chem. C* **2010**, *114*, 15924–15930.
99. Rodríguez-Sánchez, L.; Blanco, M. C.; López-Quintela, M. A. Electrochemical Synthesis of Silver Nanoparticles. *J. Phys. Chem. B* **2000**, *104*, 9683–9688.
100. Rodríguez-Vázquez, M. J.; Blanco, M. C.; Lourido, R.; Vázquez-Vázquez, C.; Pastor, E.; Planes, G. A.; Rivas, J.; López-Quintela, M. A. Synthesis of Atomic Gold Clusters with Strong Electrocatalytic Activities. *Langmuir* **2008**, *24*, 12690–12694.
101. Renjith, A.; Lakshminarayanan, V. Single-Step Electrochemical Synthesis of Cobalt Nanoclusters Embedded on Dense Graphite Sheets for Electrocatalysis of the Oxygen Evolution Reaction. *ACS Appl. Nano Mater.* **2020**, *3*, 2705–2712.
102. Zhao, M.; Sun, L.; Crooks, R. M. Preparation of Cu Nanoclusters within Dendrimer Templates. *J. Am. Chem. Soc.* **1998**, *120*, 4877–4878.

103. Yamamoto, K.; Imaoka, T.; Tanabe, M.; Kambe, T. New Horizon of Nanoparticle and Cluster Catalysis with Dendrimers. *Chem. Rev.* **2020**, *120*, 1397–1437.
104. Balogh, L.; Tomalia, D. A. Poly(Amidoamine) Dendrimer-Templated Nanocomposites. 1. Synthesis of Zerovalent Copper Nanoclusters. *J. Am. Chem. Soc.* **1998**, *120*, 7355–7356.
105. Zheng, J.; Dickson, R. M. Individual Water-Soluble Dendrimer-Encapsulated Silver Nanodot Fluorescence. *J. Am. Chem. Soc.* **2002**, *124*, 13982–13983.
106. Petty, J. T.; Zheng, J.; Hud, N. V.; Dickson, R. M. DNA-Templated Ag Nanocluster Formation. *J. Am. Chem. Soc.* **2004**, *126*, 5207–5212.
107. Xie, J.; Zheng, Y.; Ying, J. Y. Protein-Directed Synthesis of Highly Fluorescent Gold Nanoclusters. *J. Am. Chem. Soc.* **2009**, *131*, 888–889.
108. Zhang, J.; Xu, S.; Kumacheva, E. Photogeneration of Fluorescent Silver Nanoclusters in Polymer Microgels. *Adv. Mater* **2005**, *15*, 2336–2340.
109. Zhang, J.; Xu, S.; Kumacheva, E. Polymer Microgels: Reactors for Semiconductor, Metal, and Magnetic Nanoparticles. *J. Am. Chem. Soc.* **2004**, *126*, 7908–7914.
110. Shen, Z.; Duan, H.; Frey, H. Water-Soluble Fluorescent Ag Nanoclusters Obtained from Multiarm Star Poly(acrylic acid) as "Molecular Hydrogel" Templates. *Adv. Mater.* **2007**, *19*, 349–352.
111. Li, H.; Li, Z.; Wu, L.; Liu, F.; Zhou, J.; Luan, M.; Yu, M.; Wei, L. Water-soluble starlike poly(acrylic acid) graft polymer: preparation and application as templates for silver nanoclusters. *Polym. Bull.* **2012**, *68*, 2229–2242.
112. Li, L.; Li, Z.; Zhang, H.; Zhang, S.; Majeed, I.; Tan, B. Effect of Polymer Ligand Structures on Fluorescence of Gold Clusters Prepared by Photoreduction. *Nanoscale* **2013**, *5*, 1986–1992.
113. Hu, D.; Jin, S.; Shi, Y.; Wang, X.; Graff, R. W.; Liu, W.; Zhu, M.; Gao, H. Preparation of Hyperstar Polymers with Encapsulated $Au_{25}(SR)_{18}$ Clusters as Recyclable Catalysts for Nitrophenol Reduction. *Nanoscale* **2017**, *9*, 3629–3636.
114. Corbierre, M. K.; Cameron, N. S.; Sutton, M.; Mochrie, S. G. J.; Lurio, L. B.; Rühm, A.; Lennox, R. B. Polymer-Stabilized Gold Nanoparticles and Their Incorporation into Polymer Matrices. *J. Am. Chem. Soc.* **2001**, *123*, 10411–10412.
115. Patel, A. S.; Sahoo, H.; Mohanty, T. Probing the Förster Resonance Energy Transfer between Fluorescent Copper Nanoclusters and Cobalt Complex. *Appl. Phys. Lett.* **2014**, *105*, 063112.
116. Zhou, Y.; Zeng, H. C. Simultaneous Synthesis and Assembly of Noble Metal Nanoclusters with Variable Micellar Templates. *J. Am. Chem. Soc.* **2014**, *136*, 13805–13817.
117. Chandler, M.; Shevchenko, O.; Vivero-Escoto, J. L.; Striplin, C. D.; Afonin, K. A. DNA-Templated Synthesis of Fluorescent Silver Nanoclusters. *J. Chem. Educ.* [Online early access]. DOI: 10.1021/acs.jchemed.0c00158. Published online Jun 10, 2020. https://doi.org/10.1021/acs.jchemed.0c00158.
118. Chen, Y.; Phipps, M. L.; Werner, J. H.; Chakraborty, S.; Martinez, J. S. DNA Templated Metal Nanoclusters: From Emergent Properties to Unique Applications. *Acc. Chem. Res.* **2018**, *51*, 2756–2763.
119. Qiao, B.; Wang, A.; Yang, X.; Allard, L. F.; Jiang, Z.; Cui, Y.; Liu, J.; Li, J.; Zhang, T. Single-Atom Catalysis of CO Oxidation Using $Pt_1/FeO_x$. *Nat. Chem.* **2011**, *3*, 634–641.

120. Lin, J.; Wang, A.; Qiao, B.; Liu, X.; Yang, X.; Wang, X.; Liang, J.; Li, J.; Liu, J.; Zhang, T. Remarkable Performance of $Ir_1/FeO_x$ Single-Atom Catalyst in Water Gas Shift Reaction. *J. Am. Chem. Soc.* **2013**, *135*, 15314–15317.
121. Liu, L.; Lin, X.-X.; Zou, S.-Y.; Wang, A.-J.; Chen, J.-R.; Feng, J.-J. One-Pot Wet-Chemical Synthesis of PtPd@Pt Nanocrystals Supported on Reduced Graphene Oxide with Highly Electrocatalytic Performance for Ethylene Glycol Oxidation. *Electrochim. Acta* **2016**, *187*, 576–583.
122. Hackett, S. F. J.; Brydson, R. M.; Gass, M. H.; Harvey, I.; Newman, A. D.; Wilson, K.; Lee, A. F. High-Activity, Single-Site Mesoporous $Pd/Al_2O_3$ Catalysts for Selective Aerobic Oxidation of Allylic Alcohols. *Angew. Chem., Int. Ed.* **2007**, *46*, 8593–8596.
123. Zhang, X.; Shi, H.; Xu, B.-Q. Catalysis by Gold: Isolated Surface $Au^{3+}$ Ions are Active Sites for Selective Hydrogenation of 1,3-Butadiene over $Au/ZrO_2$ Catalysts. *Angew. Chem., Int. Ed.* **2005**, *44*, 7132–7135.
124. Li, H.; Wang, L.; Dai, Y.; Pu, Z.; Lao, Z.; Chen, Y.; Wang, M.; Zheng, X.; Zhu, J.; Zhang, W.; Si, R.; Ma, C.; Zeng, J. Synergetic Interaction between Neighbouring Platinum Monomers in $CO_2$ Hydrogenation. *Nat. Nanotechnol.* **2018**, *13*, 411–417.
125. Sharma, P.; Sharma, R. K. Platinum Functionalized Multiwall Carbon Nanotube Composites as Recyclable Catalyst for Highly Efficient Asymmetric Hydrogenation of Methyl Pyruvate. *RSC Adv.* **2015**, *5*, 102481–102487.
126. Sharma, P.; Solanki, M.; Sharma, R. K. Metal-Functionalized Carbon Nanotubes for Biomass Conversion: Base-Free Highly Efficient and Recyclable Catalysts for Aerobic Oxidation of 5-Hydroxymethylfurfural. *New J. Chem.* **2019**, *43*, 10601–10609.
127. Choi, C. H.; Kim, M.; Kwon, H. C.; Cho, S. J.; Yun, S.; Kim, H.-T.; Mayrhofer, K. J. J.; Kim, H.; Choi, M. Tuning Selectivity of Electrochemical Reactions by Atomically Dispersed Platinum Catalyst. *Nat. Commun.* **2016**, *7*, 10922.
128. Wang, X.; Chen, X.; Thomas, A.; Fu, X.; Antonietti, M. Metal-Containing Carbon Nitride Compounds: A New Functional Organic–Metal Hybrid Material. *Adv. Mater.* **2009**, *21*, 1609–1612.
129. Rao, T. U. B.; Nataraju, B.; Pradeep, T. $Ag_9$ Quantum Cluster through a Solid-State Route. *J. Am. Chem. Soc.* **2010**, *132*, 16304–16307.
130. Ishida, T.; Kawakita, N.; Akita, T.; Haruta, M. One-Pot *N*-Alkylation of Primary Amines to Secondary Amines by Gold Clusters Supported on Porous Coordination Polymers. *Gold Bull.* **2009**, *42*, 267–274.
131. Murugadoss, A.; Kai, N.; Sakurai, H. Synthesis of Bimetallic Gold–Silver Alloy Nanoclusters by Simple Mortar Grinding. *Nanoscale* **2012**, *4*, 1280–1282.
132. Liu, Q.; Wang, X.; Ren, Y.; Yang, X.; Wu, Z.; Liu, X.; Li, L.; Miao, S.; Su, Y.; Li, Y.; Liang, C.; Huang, Y. Synthesis of Subnanometer-Sized Gold Clusters by a Simple Milling-Mediated Solid Reduction Method. *Chin. J. Chem.* **2018**, *36*, 329–332.
133. Shao, C.; Yuan, B.; Wang, H.; Zhou, Q.; Li, Y.; Guan, Y.; Deng, Z. Eggshell Membrane as a Multimodal Solid State Platform for Generating Fluorescent Metal Nanoclusters. *J. Mater. Chem.* **2011**, *21*, 2863–2866.

134. Duan, H.; Nie, S. Etching Colloidal Gold Nanocrystals with Hyperbranched and Multivalent Polymers: A New Route to Fluorescent and Water-Soluble Atomic Clusters. *J. Am. Chem. Soc.* **2007**, *129*, 2412–2413.
135. Qian, H.; Zhu, M.; Lanni, E.; Zhu, Y.; Bier, M. E.; Jin, R. Conversion of Polydisperse Au Nanoparticles into Monodisperse $Au_{25}$ Nanorods and Nanospheres. *J. Phys. Chem. C* **2009**, *122*, 17599–17603.
136. Lin, C.-A. J.; Yang, T.-Y.; Lee, C.-H.; Huang, S. H.; Sperling, R. A.; Zanella, M.; Li, J. K.; Shen, J.-L.; Wang, H.-H.; Yeh, H.-I.; Parak, W. J.; Chang, W. H. Synthesis, Characterization, and Bioconjugation of Fluorescent Gold Nanoclusters toward Biological Labeling Applications. *ACS Nano* **2009**, *3*, 395–401.
137. Nasaruddin, R. R.; Chen, T.; Yan, N.; Xie, J. Roles of Thiolate Ligands in the Synthesis, Properties and Catalytic Application of Gold Nanoclusters. *Coord. Chem. Rev.* **2018**, *368*, 60–79.
138. Jin, R.; Zeng, C.; Zhou, M.; Chen, Y. Atomically Precise Colloidal Metal Nanoclusters and Nanoparticles: Fundamentals and Opportunities. *Chem. Rev.* **2016**, *116*, 10346–10413.
139. Zeng, C.; Li, T.; Das, A.; Rosi, N. L.; Jin, R. Chiral Structure of Thiolate-Protected 28-Gold-Atom Nanocluster Determined by X-ray Crystallography. *J. Am. Chem. Soc.* **2013**, *135*, 10011–10013.
140. Zeng, C.; Qian, H.; Li, T.; Li, G.; Rosi, N. L.; Yoon, B.; Barnett, R. N.; Whetten, R. L.; Landman, U.; Jin, R. Total Structure and Electronic Properties of the Gold Nanocrystal $Au_{36}(SR)_{24}$. *Angew. Chem., Int. Ed.* **2012**, *51*, 13114–13118.
141. Zeng, C.; Liu, C.; Chen, Y.; Rosi, N. L.; Jin, R. Gold–Thiolate Ring as a Protecting Motif in the $Au_{20}(SR)_{16}$ Nanocluster and Implications. *J. Am. Chem. Soc.* **2014**, *136*, 11922–11925.
142. Zeng, C.; Chen, Y.; Kirschbaum, K.; Appavoo, K.; Sfeir, M. Y.; Jin, R. Structural Patterns at All Scales in a Nonmetallic Chiral $Au_{133}(SR)_{52}$ Nanoparticle. *Sci. Adv.* **2015**, *1*, e1500045.
143. Das, A.; Li, T.; Li, G.; Nobusada, K.; Zeng, C.; Rosi, N. L.; Jin, R. Crystal Structure and Electronic Properties of a Thiolate-Protected $Au_{24}$ Nanocluster. *Nanoscale* **2014**, *6*, 6458–6462.
144. Zeng, C.; Liu, C.; Chen, Y.; Rosi, N. L.; Jin, R. Atomic Structure of Self-Assembled Monolayer of Thiolates on a Tetragonal $Au_{92}$ Nanocrystal. *J. Am. Chem. Soc.* **2016**, *138*, 8710–8713.
145. Kang, X.; Zhou, M.; Wang, S.; Jin, S.; Sun, G.; Zhu, M.; Jin, R. The Tetrahedral Structure and Luminescence Properties of Bi-Metallic $Pt_1Ag_{28}(SR)_{18}(PPh_3)_4$ Nanocluster. *Chem. Sci.* **2017**, *8*, 2581–2587.
146. Xu, Q.; Wang, S.; Liu, Z.; Xu, G.; Meng, X.; Zhu, M. Synthesis of Selenolate-Protected $Au_{18}(SeC_6H_5)_{14}$ Nanoclusters. *Nanoscale* **2013**, *5*, 1176–1182.
147. Zeng, C.; Liu, C.; Pei, Y.; Jin, R. Thiol Ligand-Induced Transformation of $Au_{38}(SC_2H_4Ph)_{24}$ to $Au_{36}(SPh\text{-}t\text{-}Bu)_{24}$. *ACS Nano* **2013**, *7*, 6138–6145.
148. Li, Q.; Taylor, M. G.; Kirschbaum, K.; Lambright, K. J.; Zhu, X.; Mpourmpakis, G.; Jin, R. Site-Selective Substitution of Gold Atoms in the $Au_{24}(SR)_{20}$ Nanocluster by Silver. *J. Colloid Interface Sci.* **2017**, *505*, 1202–1207.

149. Fan, J.; Song, Y.; Chai, J.; Yang, S.; Chen, T.; Rao, B.; Yu, H.; Zhu, M. The Solely Motif-Doped $Au_{36-x}Ag_x(SPh\text{-}tBu)_{24}$ ($x$ = 1–8) Nanoclusters: X-ray Crystal Structure and Optical Properties. *Nanoscale* **2016**, *8*, 15317–15322.
150. Chai, J.; Lv, Y.; Yang, S.; Song, Y.; Zan, X.; Li, Q.; Yu, H.; Wu, M.; Zhu, M. X-ray Crystal Structure and Optical Properties of $Au_{38-x}Cu_x(2,4\text{-}(CH_3)_2C_6H_3S)_{24}$ ($x$ = 0–6) Alloy Nanocluster. *J. Phys. Chem. C* **2017**, *121*, 21665–21669.
151. Yang, S.; Chai, J.; Song, Y.; Fan, J.; Chen, T.; Wang, S.; Yu, H.; Li, X.; Zhu, M. In Situ Two-Phase Ligand Exchange: A New Method for the Synthesis of Alloy Nanoclusters with Precise Atomic Structures. *J. Am. Chem. Soc.* **2017**, *139*, 5668–5671.
152. Song, Y.; Jin, S.; Kang, X.; Xiang, J.; Deng, H.; Yu, H.; Zhu, M. How a Single Electron Affects the Properties of the "Non-Superatom" $Au_{25}$ Nanoclusters. *Chem. Mater.* **2016**, *28*, 2609–2617.
153. Zan, X.; Li, Q.; Pan, Y.; Morris, D. J.; Zhang, P.; Li, P.; Yu, H.; Zhu, M. Versatile Ligand-Exchange Method for the Synthesis of Water-Soluble Monodisperse AuAg Nanoclusters for Cancer Therapy. *ACS Appl. Nano Mater.* **2018**, *1*, 6773–6781.
154. Kang, X.; Zhu, M. Transformation of Atomically Precise Nanoclusters by Ligand-Exchange. *Chem. Mater.* **2019**, *31*, 9939–9969.
155. Wiebenga, M. H.; Kim, C. H.; Schmieg, S. J.; Oh, S. H.; Brown, D. B.; Kim, D. H.; Lee, J.-H.; Peden, C. H. F. Deactivation Mechanisms of Pt/Pd-Based Diesel Oxidation Catalysts. *Catal. Today* **2012**, *184*, 197–204.
156. Graham, G. W.; Jen, H. W.; Ezekoye, O.; Kudla, R. J.; Chun, W.; Pan, X. Q.; McCabe, R. W. Effect of Alloy Composition on Dispersion Stability and Catalytic Activity for NO Oxidation over Alumina-Supported Pt–Pd Catalysts. *Catal. Lett.* **2007**, *116*, 1–8.
157. Carrillo, C.; Johns, T. R.; Xiong, H.; DeLaRiva, A.; Challa, S. R.; Goeke, R. S.; Artyushkova, K.; Li, W.; Kim, C. H.; Datye, A. K. Trapping of Mobile Pt Species by PdO Nanoparticles under Oxidizing Conditions. *J. Phys. Chem. Lett.* **2014**, *5*, 2089–2093.
158. Jones, J.; Xiong, H.; DeLaRiva, A. T.; Peterson, E. J.; Pham, H.; Challa, S. R.; Qi, G.; Oh, S.; Wiebenga, M. H.; Pereira Hernández, X. I.; Wang, Y.; Datye, A. K. Thermally Stable Single-Atom Platinum-on–Ceria Catalysts via Atom Trapping. *Science* **2016**, *353*, 150.
159. Xiong, H.; Lin, S.; Goetze, J.; Pletcher, P.; Guo, H.; Kovarik, L.; Artyushkova, K.; Weckhuysen, B. M.; Datye, A. K. Thermally Stable and Regenerable Platinum–Tin Clusters for Propane Dehydrogenation Prepared by Atom Trapping on Ceria. *Angew. Chem., Int. Ed.* **2017**, *54*, 8986–8991.